

**DEVELOPMENT OF SURFACE SURVEILLANCE SYSTEM USING
AUTONOMOUS DRONES**

LIM WEN QING


**A project report submitted in partial fulfilment of the
requirements for the award of Bachelor of Engineering
(Honours) Mechatronics Engineering**

**Lee Kong Chian Faculty of Engineering and Science
Universiti Tunku Abdul Rahman**

April 2021

DECLARATION

I hereby declare that this project report is based on my original work except for citations and quotations which have been duly acknowledged. I also declare that it has not been previously and concurrently submitted for any other degree or award at UTAR or other institutions.

Signature : 

Name : LIM WEN QING

ID No. : 1605635

Date : 18 April 2021

APPROVAL FOR SUBMISSION

I certify that this project report entitled “**DEVELOPMENT OF SURFACE SURVEILLANCE SYSTEM USING AUTONOMOUS DRONES**” was prepared by **LIM WEN QING** has met the required standard for submission in partial fulfilment of the requirements for the award of Bachelor of Engineering (Honours) Mechatronic Engineering at Universiti Tunku Abdul Rahman.

Approved by,

Signature :  _____

Supervisor : Danny Ng

Date : 19/4/21

Signature : _____

Co-Supervisor : _____

Date : _____

The copyright of this report belongs to the author under the terms of the copyright Act 1987 as qualified by Intellectual Property Policy of Universiti Tunku Abdul Rahman. Due acknowledgement shall always be made of the use of any material contained in, or derived from, this report.

© 2021, LIM WEN QING. All right reserved.

ACKNOWLEDGEMENTS

Foremost, I would like to thank everyone who had contributed to the successful completion of this project. I would like to express my deep and sincere gratitude to my research supervisor, IR. Danny Ng Wee Kiat for his guidance, motivation, invaluable advice and his enormous patience throughout the development of the research. It was a great privilege and honour to work and study under his guidance.

In addition, I would also like to express my gratitude to my loving parents and friends who had helped and given me encouragement in the journey of this research. Furthermore, special thanks to all the staff in the department of safety and security UTAR Kampar Campus (DSS-KPR) for their help and cooperation.

ABSTRACT

The development of drones is significant in the past few years. Drones are more reliable and common now. People started to realise their potential and used it in the surveillance industry. Universiti Tunku Abdul Rahman (UTAR) Kampar had decided to use drones for the surveillance land owned by UTAR to prevent unauthorised construction and plantation. “DJI Mavic 2 Enterprise Dual” is selected and responsible for the mapping mission via DJI Pilot. A total of 1741 images are captured to reconstruct the two-dimensional (2D) and three-dimensional (3D) map of the rural area which is owned by UTAR. An automated image sorting system is created to sort the images due to their large size and repeatability. The reconstruction of images is carried out by WebODM. The custom parameters for the reconstruction are dem-resolution: 15, ignore-gsd: true, min-num-features: 20000, orthophoto-resolution: 15, skip-3dmodel: true, texturing-data-term: area. It is specifically built for the reconstruction of the area, which is full of trees and green vegetation. 2D map is a digital orthophoto map (DOM). These images covered an area of around 1 971 000 Sq Meters (488 Acres). After obtaining the 2D map, the 2D map in different timestamps will be used to compare and find out the difference to achieve the objective of surface surveillance. This process is known as change detection. The change detection is done by image registration followed by principal component analysis (PCA) and K-mean clustering on the “difference image” to cluster out changes and non-changes. A cluster of four is used for the K-mean clustering to minimise the noises and false-positive detection.

TABLE OF CONTENTS

DECLARATION		i
APPROVAL FOR SUBMISSION		ii
ACKNOWLEDGEMENTS		iv
ABSTRACT		v
TABLE OF CONTENTS		vi
LIST OF TABLES		viii
LIST OF FIGURES		ix
LIST OF SYMBOLS / ABBREVIATIONS		xiii
LIST OF APPENDICES		xv
 CHAPTER		
1	INTRODUCTION	1
	1.1 General Introduction	1
	1.1.1 Drone	1
	1.1.2 Surveillance System	1
	1.2 Problem Statement	2
	1.3 Aim and Objectives	3
	1.4 Scope and Limitation of the Study	3
	1.5 Contribution of the Study	4
	1.6 Outline of the Report	4
2	LITERATURE REVIEW	5
	2.1 Drone	5
	2.1.1 Multi-rotor	5
	2.1.2 Fixed-wing	6
	2.1.3 Comparison	8
	2.2 2D and 3D Map Reconstruction	9
	2.2.1 Structure from Motion (SFM)	9
	2.2.2 Multi-view Stereo (MVS)	10
	2.2.3 3D Model	11
	2.2.4 DOM	12
	2.2.5 Available Software	13
	2.3 Change Detection	14

	2.3.1	Object-Based Hierarchical Method (OBIA)	14
	2.3.2	M-DSM Change Detection Method	17
	2.3.3	Edge Detection Based Method	18
	2.3.4	Region Growing Algorithm Based Method	19
	2.3.5	PCA and K-means Clustering Method	23
3		METHODOLOGY AND WORK PLAN	26
	3.1	Project Flow	26
	3.2	Mapping	28
	3.3	Sort and Transfer Images	29
	3.4	WebODM	32
	3.4.1	Ignore-gsd	34
	3.4.2	Dem-resolution	35
	3.4.3	Orthophoto-resolution	35
	3.4.4	Min-num-features	35
	3.4.5	Skip-3dmodel	35
	3.4.6	Texturing-data-term	36
	3.5	Change Detection	36
	3.5.1	Realign Orthophoto	37
	3.5.2	Remove Black Spot	38
	3.5.3	Pre-processing	39
	3.5.4	Image 1 – Image 2	40
	3.5.5	PCA and K-Means Clustering	40
	3.5.6	Post-processing	41
4		RESULTS AND DISCUSSIONS	44
	4.1	WebODM Results	44
	4.1.1	Parameters	44
	4.1.2	Orthophotos and 3D Points Cloud	47
	4.2	Change Detection Results	49
5		CONCLUSIONS AND RECOMMENDATIONS	58
	5.1	Conclusions	58
	5.2	Recommendations for Future Work	59
		REFERENCES	60
		APPENDICES	64

LIST OF TABLES

Table 2.1:	Advantages and Disadvantages of Multi-rotor Drones.	6
Table 2.2:	Advantages and Disadvantages of Fixed-wing Drones.	7
Table 2.3:	Evaluation of Multi-rotor Drone and Fixed-wing Drone.	8

LIST OF FIGURES

Figure 2.1:	DJI Mavic 2 Pro Quadcopter (DJI, 2020).	5
Figure 2.2:	AgEagle RX-48 Fixed-Wing Drone (DronesWatch, 2020).	7
Figure 2.3:	Steps of DOM Formation.	9
Figure 2.4:	Illustration of SFM (Toffanin, 2019).	10
Figure 2.5:	Formation of a Dense Point Cloud (Kar, 2017).	11
Figure 2.6:	Dense Point Cloud (Toffanin, 2019).	11
Figure 2.7:	Polygonal Mesh (Toffanin, 2019).	12
Figure 2.8:	Textured Mesh (Toffanin, 2019).	12
Figure 2.9:	Orthographic Camera Taking a Picture of 3D Model form Top (Toffanin, 2019).	13
Figure 2.10:	DOM (Toffanin, 2019).	13
Figure 2.11:	Primitive Segmentations and Multi-Primitive Segmentations: First row: left to right: ortho-images of one date, TS and DB; Second row, left to right: BB, CS and BO; Third row: TDBCB, TDB and TC (Qin, 2014).	16
Figure 2.12:	Workflow of Multi-Criteria Decision Analysis.	16
Figure 2.13:	Workflow of M-DSM Method.	18
Figure 2.14:	Illustration of Edge Detection Based Change Detection Algorithm. (Top left) Image 1. (Top right) Image 2. (Bottom left) Edge detection. (Bottom right) Feature extraction (Ugliano <i>et al.</i> , 2015).	19
Figure 2.15:	Processing Chain of Region Growing Algorithm Based Method.	20
Figure 2.16:	Steps of Automatic Noise Reduction Method.	21
Figure 2.17:	Steps of Threshold Range Prediction (TRP).	22
Figure 2.18:	Illustration of mRGA.	22
Figure 2.19:	Workflow of PCA and K-means Clustering Method.	23

Figure 2.20:	Comparison of Change Detection Results. (a) Input image 1. (b) Input image 2. (c) EM-based thresholding. (d) MRF-based thresholding. (e) PCA K-means Clustering.	24
Figure 2.21:	Detection performance comparisons against different levels of noises. (a) Zero-mean Gaussian Noise. (b) Speckle noise.	24
Figure 3.1:	Project Flow Chart.	26
Figure 3.2:	DJI Mavic 2 Enterprise Dual.	27
Figure 3.3:	Mapping Mission by using DJI Pilot.	27
Figure 3.4:	Batch File with Two Options.	28
Figure 3.5:	Lands Owned by UTAR.	29
Figure 3.6:	After Select Option One.	30
Figure 3.7:	Mean of Coordinates for Each Plot.	31
Figure 3.8:	Option Two.	31
Figure 3.9:	Click “Select Images and GCP” to upload images.	32
Figure 3.10:	Select images and press “Open”.	33
Figure 3.11:	Name the tasks accordingly, choose option “UTAR_Kampar” and click “Preview”.	33
Figure 3.12:	Click “Start Processing”.	34
Figure 3.13:	Leave the webpage open until the uploading process is completed.	34
Figure 3.14:	User Interface for Change Detection.	36
Figure 3.15:	User Interface of Change Detection After Selected Two Images.	37
Figure 3.16:	Flow Chart of Change Detection.	38
Figure 3.17:	Illustration of the Realignment of DOM.	38
Figure 3.18:	DOM Before Realignment.	39
Figure 3.19:	DOM After Realignment.	39
Figure 3.20:	DOM After Pre-processing.	40

Figure 3.21: Difference Image.	40
Figure 3.22: Binary Change Map.	41
Figure 3.23: Change Map After Post-processing.	42
Figure 3.24: Orthophoto 1 with Highlighted Changes.	42
Figure 3.25: Orthophoto 2 with Highlighted Changes.	43
Figure 4.1: Flight Map of the Kuala Selangor Rural Area.	44
Figure 4.2: Default Orthophoto.	45
Figure 4.3: High-Resolution Orthophoto.	45
Figure 4.4: Forest Orthophoto.	46
Figure 4.5: Custom Parameter Orthophoto for UTAR Kampar Area.	46
Figure 4.6: Plot_A Orthophoto.	47
Figure 4.7: Plot_BC Orthophoto.	48
Figure 4.8: Plot_A 3D Points Cloud.	48
Figure 4.9: Plot_BC 3D Points Cloud.	49
Figure 4.10: Orthophotos of Toufen, 11 th Apr 2019 (Left) 16 th Sept 2019 (Right).	49
Figure 4.11: Change Map when the Number of Clusters is Two.	50
Figure 4.12: Change Map when the Number of Clusters is Three.	51
Figure 4.13: Change Map when the Number of Clusters is Four.	51
Figure 4.14: Change Map when the Number of Clusters is Five.	52
Figure 4.15: Orthophoto 1 with Highlighted Changes.	52
Figure 4.16: Orthophoto 2 with Highlighted Changes.	53
Figure 4.17: Cropped Image from 11 th April (Left) and 16 th Sept (Right).	53
Figure 4.18: Edited Orthophoto of Plot_BC.	54
Figure 4.19: Plot_BC Edited Orthophoto with Highlighted Changes.	55

- Figure 4.20: Kuala Selangor Change Map of 14th January and 15th January. 55
- Figure 4.21: Kuala Selangor Change Map of 14th January and 17th January. 56
- Figure 4.22: Cropped Image from 14th January (Left) and 17th January (Right). 56
- Figure 4.23: New Change Map by “Bitwise And” Operation. 57

LIST OF SYMBOLS / ABBREVIATIONS

r	gaussian filter radius
T	predicted binary threshold
T_{hei}	threshold of height different
T_{elong}	threshold of elongation
T_{convex}	threshold of convex
2D	two-dimensional
3D	three-dimensional
BA	bundle adjustment
BB	bring blobs
BCDM	binary change detection map
BO	blob-shaped objects
CCTV	closed-circuit television
CI	credible interval
CMI	change magnitude image
CS	connected surface segments
DB	dark blobs
DOM	digital orthophoto map
DSM	digital surface model
DTM	digital terrain model
EM	expectation maximisation
FCMI	filtered change magnitude image
GCPs	ground control points
GF	Gaussian filter
IGR	initial growing region
MLS	moving least squares
MRF	Markov random fields
mRGA	modified regional growing algorithm
MVS	multi view stereo
nEGI	excessive green index
OBIA	object-based image analysis
ODM	open drone map

ORB	oriented brief
PCA	principal component analysis
PSNR	peak signal-to-noise ratio
RSFCM	robust semi-supervised fuzzy C-means
SFM	structure from motion
THR	top-hat reconstruction
TRP	threshold range prediction
TS	texture segments
UAV	unmanned aerial vehicle
UTAR	Universiti Tunku Abdul Rahman

LIST OF APPENDICES

APPENDIX A: DJI Mavic 2 Enterprise Dual Specification	64
APPENDIX B: Flight Plans of the Drone	72
APPENDIX C: Flight Planning of Operation Area	78

CHAPTER 1

INTRODUCTION

1.1 General Introduction

1.1.1 Drone

Unmanned Aerial Vehicle (UAV) is an aircraft without a human pilot on board. UAV is commonly known as a drone. These two terms have become interchangeable. The development of UAVs is significant in the past few years. UAVs are more reliable and common now. People start to realise their potential. Usages of UAVs can be divided into six categories: Research and development, Logistics, Target and decoy, Combat, Reconnaissance, and Civil and commercial.

Years before 2010, UAV was mainly used in the military sector to carry out missions that are too dangerous for humans. It is built for combat and reconnaissance. Back in 1916, the first UAV named “Ruston Proctor Aerial Target” was developed after the outbreak of world war one. This military UAV used a radio system as guidance (Tan et al., 2020). Today, UAVs have expanded far beyond military applications. UAVs have become prevalent in aerial photography, product deliveries, policing, agriculture, surveillance, infrastructure inspections, and others.

There are mainly four types of drones, single-rotor, multi-rotor, fixed-wing, and fixed-wing hybrid. Different types of drone have their own strengths and weaknesses. For example, multi-rotor drones are stable and easy to control but have limited flying time. Fixed-wing drones can fly for couples of hours, but they are costly.

1.1.2 Surveillance System

Video surveillance involves the act of observing and looking for a specific activity that is improper. The surveillance system certainly helps to deter crime. Crime is the “purposive behaviour designed to meet the offend’s commonplace needs”. The surveillance system reduces the number of criminal opportunities and increases the perceived risk of offending. It increases the risks of a particular crime and persuades the offender to abstain from crime. In the rational choice

perspective, the offender will consider the potential rewards and inherent risks involved in the commission of criminal activity (Piza et al., 2019).

In the current market, the most conventional video surveillance system is closed-circuit television (CCTV). It is commonly used for homes, stores, businesses, and banks. A single or multi-cameras, a recording device, and a monitor are the main components of a CCTV system. The system can be wired or wireless. It allows the use of cameras to monitor the exterior and interior of property by transmitting the video signal to a monitor. The function of video-recording of CCTV can help detectives to solve crimes.

One of the main problems of this system is that the vision of CCTV cameras is limited. Once the cameras are installed, they are only capable of tracking for a certain angle and area. It is not feasible to cover and surveillance on an extremely large scale area. Furthermore, it needs an uninterrupted power supply. The camera needs electricity to function. This has made surveillance in the wilderness area, which does not have basic infrastructure almost impossible.

Besides, satellite remote sensing is one of the solutions to monitor large scale areas and wildlands. However, using a satellite as a surveillance system is not feasible. The cost of satellite remote sensing is high. The resolution of the image is relatively low. According to the Malaysian Space Agency, the cost of a 60 km x 60 km with 2.5 m spatial resolution is around RM 5 400. Besides, it needs to take 1 to 2 weeks to deliver.

1.2 Problem Statement

Unauthorised construction and plantation on private lands are pretty typical in Malaysia. It is illegal and infringes on the rights of the land's owner. In addition to the potential technical hazards on uncontrolled construction sites or finished buildings, illegal construction activity can be a violation of the environment when the works invade nature reserves areas. It also increased landslide risk due to loss of stabilisation by deforestation if the construction is on hillside regions. In terms of illegal plantation, it may cause environmental problems such as soil erosion, biodiversity and pollution (Hartemink, 2005).

The consequences of these unauthorised activities are the owner of the land needed to spend money to solve the problem. Prevention is better than cure.

Therefore, a real-time surveillance system is needed. A drone is the best choice as a surveillance system when facing large scale wilderness areas.

1.3 Aim and Objectives

This project aims to create an autonomous drone to monitor an area and identify changes to the area under surveillance.

Objectives:

1. To create flight plans for the drone mapping process.
2. Carry out image reconstruction using aerial footage to create two-dimensional (2D) and three-dimensional (3D) maps.
3. Develop software to identify anomalies in the area under surveillance.

1.4 Scope and Limitation of the Study

The scope of study mainly involves the drone flight plan, 2D and 3D maps reconstruction, and change detection, which is also known as anomalies detection. The ideal setting for the flight plan is studied to prevent lousy reconstruction. The details of the 2D and 3D maps reconstruction process are also studied to select the best parameters. Besides, different methods of change detection have also been studied. Eventually, by combining all of them, a novel surface surveillance system using autonomous drones is created.

On the other hand, the limitations of the study are related to the mapping process and change detection. The drone is required to carry out 11 different flight plans to complete the mapping of the whole area of interest. This is due to the limitation of the battery power. The flight time of a fully charged battery is only around 30 minutes. Thus, the mapping mission needs to be separate. In terms of change detection, the algorithm is principal component analysis (PCA) and K-mean clustering with some image processing. Open morphology is used to decrease the number of noises and false positives, but at the same time, it may also remove the real anomalies which are small in size. In addition, the solution is unable to detect changes which have a very similar RGB value. This is because only orthophoto had been taken into account when carrying out the change detection. Furthermore, the weather condition, sun light position, and other environmental randomness will affect the orthophoto result, which will

further affect change detection. For example, the shadow of the tree may be detected by the algorithm as changes.

1.5 Contribution of the Study

There are 11 flight plans created for the rural area around UTAR Kampus. The ideal parameters for the reconstruction of 2D and 3D maps are also discovered. Besides, software for image sorting and change detection are created. The algorithm for the change detection is a novel algorithm. By combining all of these outcomes, a complete surface surveillance system using autonomous drones is developed.

1.6 Outline of the Report

This report is divided into five chapters. Firstly, Chapter 1 starts with a general introduction of drones and surveillance systems. The problem statement and objectives are also discussed in Chapter 1, with the aim of addressing the issues described in the problem statement. The scope of study is also described in Chapter 1 to elaborate the objectives in more detail, while informing the reader that the scope of the project is limited to certain events.

Secondly, Chapter 2 provides a literature review on the type of drones, 2D and 3D map reconstruction steps and methods for change detection. Detailed research, selection of solution, and literature review had been carried out in this chapter.

Next, Chapter 3 demonstrates the methodology to achieve the objectives of this project from head to toe. The methodology includes project flow, mapping, sort and transfer images, WebODM, and change detection.

In addition, Chapter 4 analyses and discusses the results of the WebODM and change detection. Parameters for the reconstruction, number of clusters for change detection, and others result will be shown in Chapter 4. Finally, Chapter 5 concludes the project itself and some recommendations are provided for future development.

CHAPTER 2

LITERATURE REVIEW

2.1 Drone

As mentioned in section 1.1.1, in the commercial market, there are four main types of drones, which are single-rotor, multi-rotor, fixed-wing, and fixed-wing hybrid. They have their advantages and disadvantages, including their suitability for specific applications. However, only multi-rotor and fixed-wing drones will be discussed because they are more common and available in the market.

2.1.1 Multi-rotor

Multi-rotor is also known as multicopters. It is the most popular type of drone equipped with two or more motors. Both professionals and hobbyists use it for photography, surveillance, and filmmaking because of its small size and ready to fly capabilities. There are many types of multi-rotor drones which are categorised by the number of motors used. For example, a two-motored multicopter is called a bi-copter. In the market, the number of motors can be up to eight motors.

The number of motors and configuration affect flight performance. The more the motor, the more the power and lift capacity, which means the drone could carry more payload. More motors also mean improvement on the redundancy in the event of motor failure. At the same time, more motors will decrease power efficiency and increase the cost of the drone (Yang et al., 2017). The most common multi-rotor drone is a quadcopter with X4 configuration. X4 configuration means four motors mounted on a symmetric frame. As shown in figure 2.1, each arm is typically 90 degrees apart.



Figure 2.1: DJI Mavic 2 Pro Quadcopter (DJI, 2020).

The multi-rotor drone is the cheapest and gives great control over the positioning of the drone. It is also the only type of drone, which is able to carry out autonomous take-off and return functions at a low cost. The downside of multi-rotor is their limited speed and endurance, making them unsuitable for aerial mapping on a large scale, long-endurance surveillance, and long-distance inspection. Although the technology is improving, multi-rotor drones are fundamentally inefficient and require much energy to withstand the gravity in order to carry them in the air (Chapman, 2016). The battery for drones is usually a Lipo battery. With the current technology level for batteries, multi-rotor drones are limited to a flight time of around 20 to 30 minutes while carrying a lightweight camera payload. Table 2.1 shows the advantages and disadvantages of multi-rotor drones.

Table 2.1: Advantages and Disadvantages of Multi-rotor Drones.

Advantages	Disadvantage
Easy to control.	Limited flying time, around 20-30 minutes.
Ability to hover.	Small payload capabilities.
It can take off and land vertically.	Most of the energy is spent to overcome gravity and stabilise in the air.
High stability.	

2.1.2 Fixed-wing

Fixed-wing drone is like a regular aeroplane which consists of one rigid wing that provides lift rather than vertical lift rotors. The fixed-wing drone is much more efficient because it only needs energy just to travel forward. No power is lost to hold them onto the air. This had made them capable of covering larger areas and loiter for a long time (Vergouw et al., 2016). Gas engines can also be used as their power source. The high density of fuel can make the fixed-wing drone able to remain in the air for 16 hours or more.



Figure 2.2: AgEagle RX-48 Fixed-Wing Drone (DronesWatch, 2020).

A fixed-wing drone's biggest drawback is its inability to hover in one place. This makes launching and landing the drone a lot trickier than a multi-rotor drone. Launching is depending on the size, and a small fixed-wing drone can launch by hand. The big drone needs a catapult launcher to get them into the air. Landing needs either a parachute, runway, or net for safe landing (Chapman, 2016).

Another downside is the control difficulty level. One reason why multi-rotor drones have become so widespread and popular is that it is easy to get started. The user may purchase a cheap quadcopter and begin training. Table 2.2 shows the advantages and disadvantages of fixed-wing drones.

Table 2.2: Advantages and Disadvantages of Fixed-wing Drones.

Advantages	Disadvantage
The average flight time is a few hours to 16 hours or more if a gas engine powers the drone.	A launcher is needed to take the drone into the air.
Capability to fly at a high altitude.	It takes training to fly them
Have the ability to carry more weight	More expensive.
	It can only move forward and cannot hover in the air.
	More difficult to land.

2.1.3 Comparison

The target of this project is to create a surface surveillance system using autonomous drones. The system needs to complete the surveillance mission without any human intervention. Therefore, the drone should be able to autonomously take off, patrol in the air, feedback real-time image, autonomous landing, and charging. Once it is full of battery, continue its mission. Based on these categories, an evaluation between the multi-rotor drone and fixed-wing drone was carried out to choose the most suitable drone.

Table 2.3: Evaluation of Multi-rotor Drone and Fixed-wing Drone.

	Multi-rotor Drone	Fixed-wing Drone
Cost	Normal	Normal
Hover	Able	Unable
Take Off	Able	Unable to take off autonomously.
Landing	Able	Very difficult to land.
Flight Time	20 to 30 minutes	Longer average flight time.

Table 2.1 shows that the multi-rotor drone is more suitable than a fixed-wing drone. The only weakness for multi-rotor drones in this project is the flight time. This problem can be solved by an autonomous charging station or autonomous battery swapping station. Specifically, “DJI Mavic 2 Enterprise Dual” had been chosen. It is a quadcopter with visible and thermal imagery. The maximum flight time is around 31 minutes. One of the reasons for choosing DJI drone is because DJI provides a software development kit, SDK for the drone. Window SDK will be used to achieve the desired output of this project. The DJI environment is also more well developed and accessible. There are a number of third-party software and open sources available for it. With these software, the mapping process of the drone will be much easier. After the mapping is completed, the drone will store the image footage of the area. The images will be further processed into 2D and 3D map to have better visualisation, and it will ease the process of change detection.

2.2 2D and 3D Map Reconstruction

When a UAV is capturing images, the camera is directly pointing perpendicular to the ground. Thus, the objects in the image will not be uniform. Objects at the edges will have a different scale for the objects in the centre. Therefore, after acquiring images from the drone, those images will further process to form a 2D and 3D map.

2D map is also known as orthophoto map. A digital orthophoto map (DOM) is a seamless image that has been geometrically corrected to display ground features in their actual ground position with a constant scale throughout the image. It is obtained by vertical parallel projection of a surface. This process is called orthorectification (Liu et al., 2018). On the other hand, 3D mapping means profiling of objects in three dimensions for real-world mapping of objects and terrains. It is basically a 3D model with georeferencing.

Going from images to 3D models and DOM is a series of incremental processes. The most common steps of DOM formation are shown in figure 2.3.

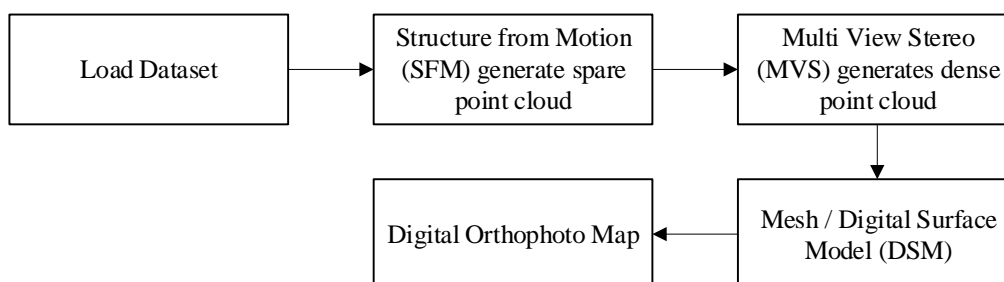


Figure 2.3: Steps of DOM Formation.

2.2.1 Structure from Motion (SFM)

SFM is a photogrammetry technique for estimating 3D structure from overlapping images. Each image is scanned for easily identifiable features such as edges, points of interest and other unique objects. Image features from one image are compared with another. When many features are shared between two images, the images are matched. After matching a single pair of images, more images were progressively added to the matching process. After that, the angle and position of the camera can be recovered for every picture. It will also generate a sparse point cloud. This information can be obtained by using perspective geometry and optics (Toffanin, 2019). The reason to use SFM to

calculate the position of the camera instead of only using the GPS information is due to GPS not being precise, and the gimbal information is not always present. SFM is much more accurate in calculating the position of the camera, and as a bonus, it does not require any GPS information at all.

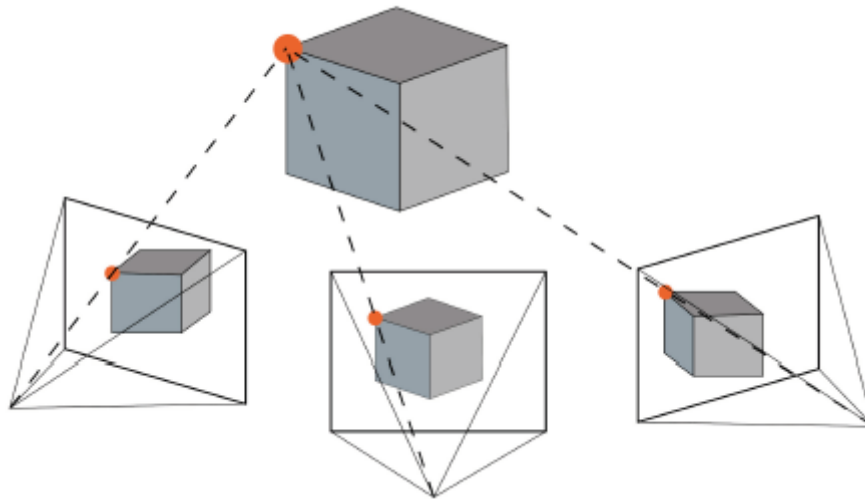


Figure 2.4: Illustration of SFM (Toffanin, 2019).

2.2.2 Multi-view Stereo (MVS)

While SFM focuses on the estimation of camera poses, MVS focuses on the reconstruction of the dense point cloud from multiple overlapping images. It will increase the density of the sparse point cloud (Gindraux, Boesch and Farinotti, 2017). The position of a 3D point can be found when two or more projection rays intersect. Therefore, the density of the dense point cloud is strongly related to the number of matching key points. In order to carry out MVS, the position and angle of cameras or as known as camera poses is needed, which had been obtained through SFM. Based on the camera poses and images, the MVS can compute out a dense point cloud. The generation of the dense point cloud is the most computationally intensive step. Some of the time, the quality of the dense point cloud is not that high and requires manual editing (Mathews, 2015).

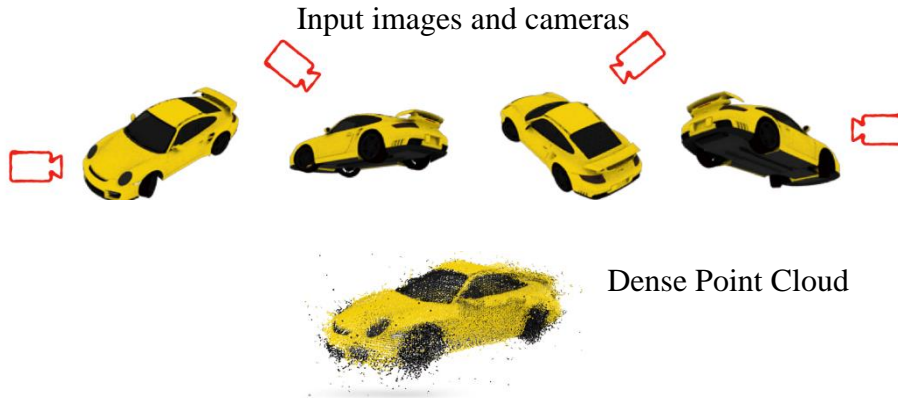


Figure 2.5: Formation of a Dense Point Cloud (Kar, 2017).

2.2.3 3D Model

After obtaining the dense point cloud, a mesh will be derived from the point cloud. More precisely, the mesh is called polygonal mesh. The 3D mesh is a geometric data structure composed of a bunch of connected triangles that define a surface explicitly. The “triangles” are formed by connecting the points in the dense point cloud (Toffanin, 2019). Therefore, the density and accuracy of the dense point cloud will affect the quality of the 3D model a lot. After having a mesh, the texturing process will be carried out. The mesh does not have any colours at this point. Texturing is the process of adding colour to the meshes. It assigns specially computed texture images to each polygon in the meshes. After the texturing process is completed. The mesh is now textured mesh which is exactly a 3D model of the captured area.

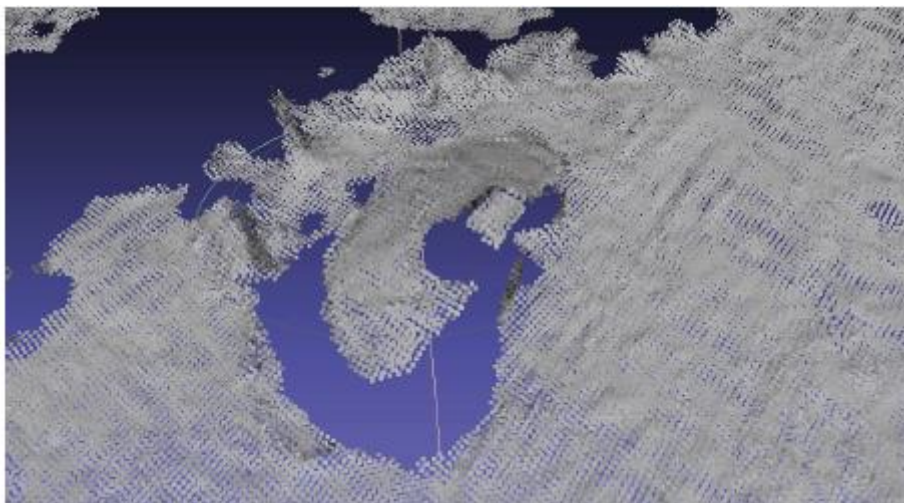


Figure 2.6: Dense Point Cloud (Toffanin, 2019).

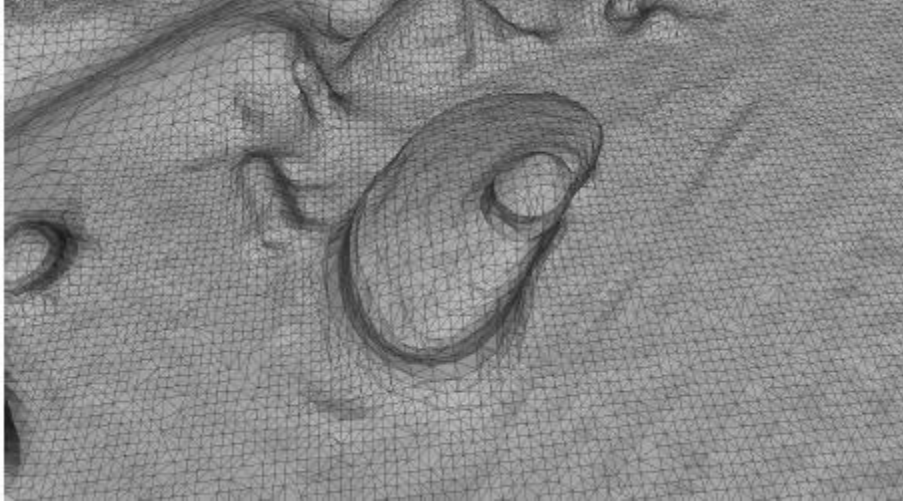


Figure 2.7: Polygonal Mesh (Toffanin, 2019).



Figure 2.8: Textured Mesh (Toffanin, 2019).

2.2.4 DOM

The goal of the DOM generation is to eliminate any distortions due to camera tilt and ground relief, thus preserving the actual dimensions of the scene or image. The DOM is generated by taking a picture of the textured 3D mesh from the top (Vacca, 2020). There are also some other methods to generate DOM, such as generating DOM from a digital surface model (DSM). Same as mesh, the DSM is generated from the dense point cloud. DSM represents the height of the features in the area of interest. In order to generate DOM, the camera's position with respect to the terrain in each captured image is used, and the images are stretched as required to correct the perspective distortions based on

the DSM and images that show better the top of the objects are selected to create a merge of all the corrected images (Stars project, n.d.).

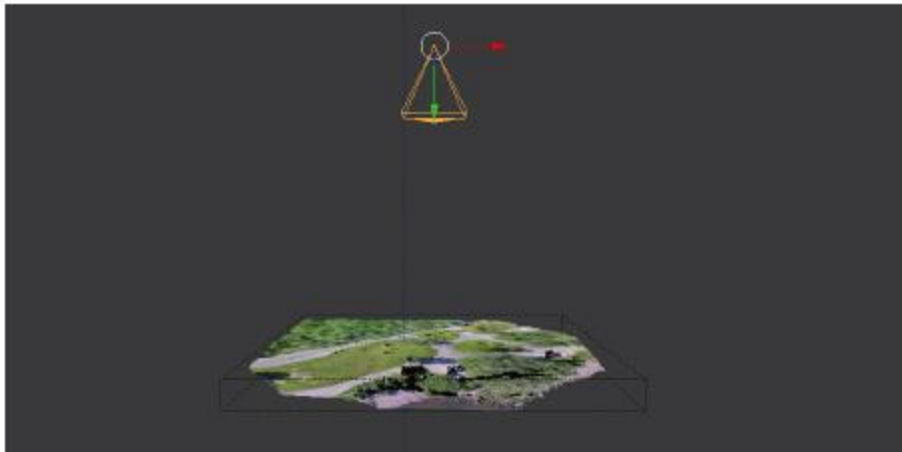


Figure 2.9: Orthographic Camera Taking a Picture of 3D Model from Top (Toffanin, 2019).



Figure 2.10: DOM (Toffanin, 2019).

2.2.5 Available Software

There is some available software built to solve these photogrammetry and UAV images reconstruction problems such as Pix4D, AgiSoft, and Drone Deploy. These software are proprietary software which usually requires license and subscription. Some open-source applications can also be used, such as Microsoft Image Composite Editor (ICE), Visual SfM and Open Drone Map (ODM).

Among these applications, Drone Deploy and ODM are exactly built for UAV imagery problems. The step for DOM generation of these two solutions is similar. The steps are stated in section 2.2.1 to 2.2.4. As mentioned, Drone Deploy is a proprietary software which required a monthly subscription of 99 dollars (Pricing & Plans | DroneDeploy, n.d.). On the other hand, ODM is totally free to use open source. Therefore, ODM is selected as the 2D and 3D map reconstruction application. After completing the reconstruction process, the DOM will be used as the raw data for change detection.

2.3 Change Detection

The change detection will be carried out after the mapping. There are quite a few approaches for detecting changes in UAV images taken at the various timestamps. Before change detection, the data needs to be registered. Registration of images is a necessary prerequisite for any algorithm of change detection. It consists of translating two images into a standard set of references. Robust and precise registration of the images from various timestamps is a crucial problem for detecting changes. Inaccurate registration will lead to incorrect change detection results. Image pre-processing is also essential. Illumination and chromatic differences always exist due to the meteorologist conditions and different positions of the sun.

2.3.1 Object-Based Hierarchical Method (OBIA)

According to Qin, 2014, a step-wise strategy had been adopted by the object-based hierarchical method under the OBIA framework. First, to reduce the geometric misalignment, registration of images of two different timestamps will be carried out under the general bundle adjustment (BA) framework. Second, a multi-primitive segmentation is accomplished based on spectral and geometric details. Third, an object-based decision tree analysis is used to detect changes.

The primitive in the multi-primitive segmentation is defined as a set of unique appearance and geometric characteristics such as blob and smoothness. Each property will create a unique primitive segmentation. The concept of multi-primitive segmentation is to combine different primitive segmentation to form a new segmentation with different properties. Change detection can be

carried out based on these segmentation results. There are three spectral primitives which are texture segments (TS), bright blobs (BB), dark blobs (DB) and two geometric primitives which are connected surface segments (CS) and blob-shaped objects (BO) are adopted in this method.

TS is formed by using efficient graph-based segmentations (EGS) (Felzenszwalb and Huttenlocher, 2004). It carries out a comparison between across-region deviations and inside-region deviations. EGS has the capability to preserve low deviation image regions while ignoring details in high deviation regions. Low deviation image regions are areas such as ground, homogenous roofs. High deviation regions are areas such as grass.

The EGS may ignore some significant small objects. Small objects such as public benches and dustbins sometimes create high local contrasts. Therefore, top-hat reconstruction (THR) is employed to extract such objects (Vincent, 1993). The DOM is transformed into CIELAB space. After that, apply the THR to the negative images and L band images. A threshold is given to truncate the computed to detect the BB and DB.

For the CS in geometric primitives, discontinuous surfaces are created by human-made structures, and the pixels on such surfaces are highly coherent in geometric deformation. A fast and straightforward 4-neighbourhood segmentation can be used to detect the large height difference with a threshold for cutting the jump of height (Davies, 2005).

Lastly, BO has a similar concept to the DB and BB. THR is applied to the DSM to detect geometric blobs. BO is complementary to the DB and BB. BO can detect the object with different height to the surroundings while they have a similar colour.

TDBCB is used in the object-based hierarchical method. TDBCB is the combination of TS, DB, BB, CS, and BO. By merging the five primitive segmentations, more detailed segmentation is created. The following operation can be carried out to merge two primitive segmentations. The equation of the TDBCB is shown below as well.

$$A \oplus B = \{C_{ij} = A_{ij} + \omega B_{ij}\}, \text{ where } \omega = \max(\{A_{ij}\})$$

$$TDBCB = TS \oplus DB \oplus BB \oplus CS \oplus BO$$

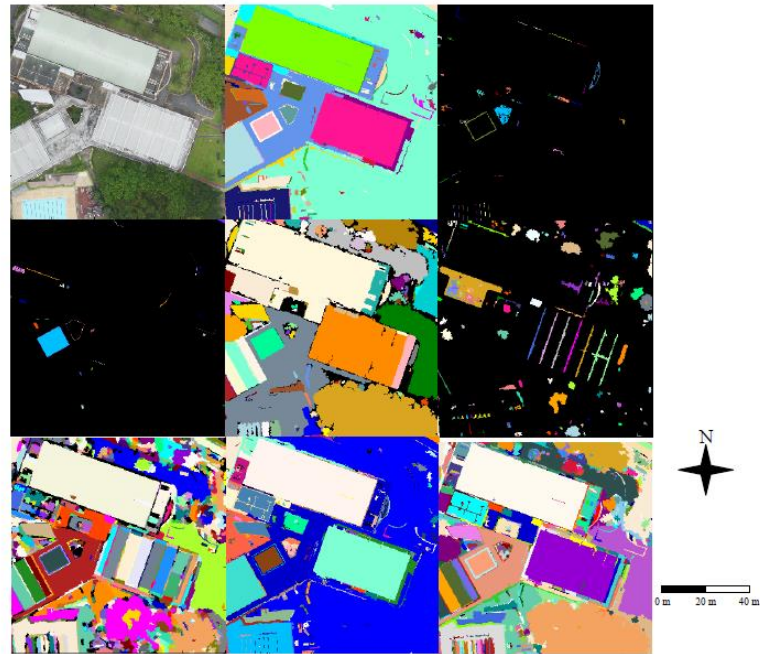


Figure 2.11: Primitive Segmentations and Multi-Primitive Segmentations (Qin, 2014): First row: left to right: ortho-images of one date, TS and DB; Second row, left to right: BB, CS and BO; Third row: TDBCBCB, TDB and TC.

After the segmentation is the decision tree analysis, the multi-criteria decision analysis process can be simplified, as shown in figure 2.12. The TDBCBCB segmentation serves as the base unit for change detection. The difference in the height of each segment in the TDBCBCB is compared to produce an initial change mask. The histogram of the elevation difference is calculated for each segment. The difference in elevation of pixels greater than 10 % of the sum is averaged out as the elevation difference value. So that a threshold, T_{hei} is given to identify segments as a potential candidate of changes.

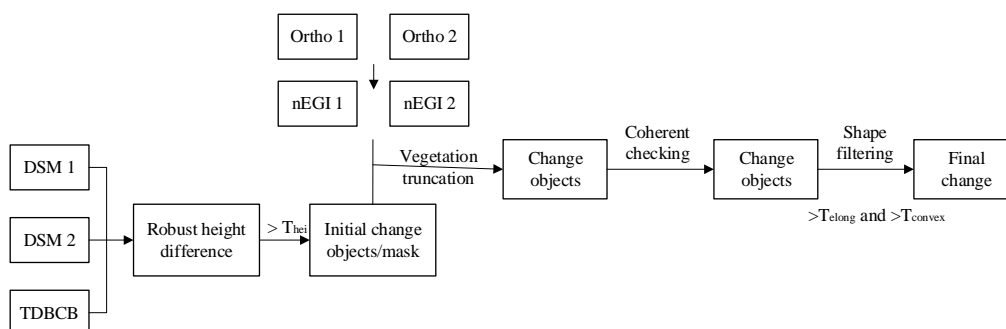


Figure 2.12: Workflow of Multi-Criteria Decision Analysis.

In change detection, the change of vegetation such as trees and grasses is not of interest. The changes are expected due to seasonal change and the irregular shapes of green vegetation. Thus, these areas are given less weight or not considered in the change analysis. The greenness of each pixel can be calculated when in the case of RGB images. It can be described by the normalised form of Excessive Green Index (nEGI) (Woebbecke et al., 1995).

$$nEGI = \frac{2G - R - B}{2G + R + B}$$

In order to remove disturbances from the green vegetation, pixels classified as green vegetation in both timestamps with elevation differences of lower than two T_{hei} and segments in TDBCB containing 80 % of such pixels will not be considered as changes.

After that, colour and smooth coherence will be carried out to get rid of the matching artefacts that usually occur at the edges of the image (Tian et al., 2013). Lastly, shape filtering will be carried out. It will consider two measures for concave and thin segments. Matching error is likely to induce some abnormal-shaped segments, such as thin structures. At the same time, small thresholds for T_{elong} and T_{convex} is used to prevent filtering the real changes (Qin, 2014).

2.3.2 M-DSM Change Detection Method

According to Xuan, 2011, a three-dimensional change detection approach is defined by comparing DSMs generated from UAV imagery from two different epochs. This approach is called the M-DSM change detection method. This method takes advantage of simplicity, versatility, security, and low cost. However, it required a high level of accuracy in the registration of the model. Thus, ground control points (GCPs) are used to increase accuracy. GCPs are points on the ground with known coordinates to assist the image reconstruction. Besides, the quality of the DSM is needed to be high and accurate as well. The algorithm is DSM of epoch two minus DSM of epoch one, which derives the differences in DSM. The difference in DSM will be further displayed on the DOM to have a better visualisation. The workflow of M-DSM is shown in figure 2.13.

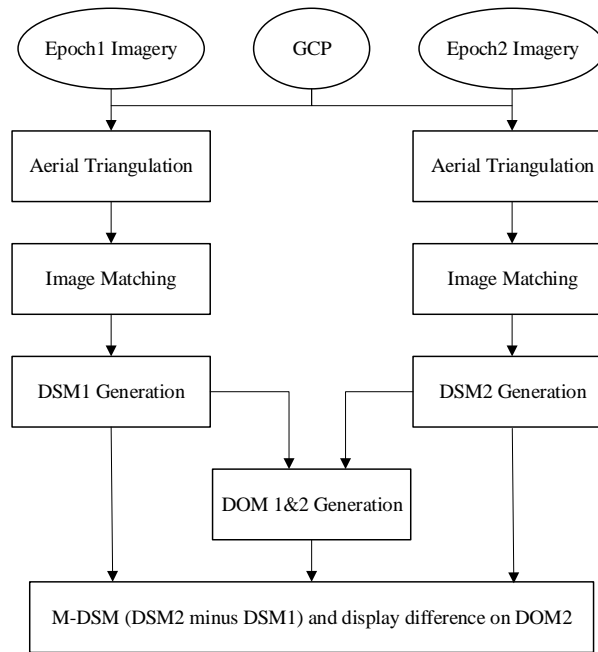


Figure 2.13: Workflow of M-DSM Method.

2.3.3 Edge Detection Based Method

According to Ugliano *et al.*, 2015, a standard image registration process is implemented in this method. It is based on the identification of image correspondence. First, it detects and extracts local features from each image through the local image descriptor Oriented BRIEF (ORB) (Rublee *et al.*, 2011). After that, these features are matched using an approximate k-Nearest Neighbor search algorithm (Muja and David Lowe, 2020) combined with a constrained random sampling consensus algorithm outliers (Fischler and Bolles, 1981) for discarding.

After registration of images, a change detection algorithm is applied to each pair of matched images. The change detection algorithm is composed of two steps. First, identifying areas inside the images where any significant changes using edge detection. The algorithm of edge detection is based on the MPEG-7 Edge Histogram Descriptor (Sikora, 2001). The RGB image is first transformed into grayscale and divided into a fine cell grid. For each cell, edge information is computed in five categories: horizontal, vertical, 45°, 135°, and unoriented. A moving window of a given size is then used to compute the total number of edges in different regions of the image. The same procedure is repeated on the second image, and the difference in the number of edges is calculated. Then,

each region where the difference exceeding a given threshold value of t_E is deemed to have been changed. In order to prevent removing real changes, a relatively low value of the threshold is preferable. This means a higher number of false positives will be obtained, which will be removed in the next step.

Second, the extraction of the feature in the detected changed area. This step is to refine the results of the first step by rejecting false positives and locating the exact position of the changes. In order to localise the changes, the ORB-based feature is computed once more time in the region flagged by the first step of the algorithm. Once located the changes, the number of false positives can be reduced by the following criterion. Since the system is searching for a permanent change rather than a fast-moving object, the changes are expected to appear in many images. Therefore, a new threshold t_F is defined, which represents the minimum percentage of images with the same coordinates where change must appear in order to be considered as an actual change. Figure 2.14 shows the illustration of the edge detection based change detection method.



Figure 2.14: Illustration of Edge Detection Based Change Detection Algorithm (Ugliano *et al.*, 2015). (Top left) Image 1. (Top right) Image 2. (Bottom left) Edge detection. (Bottom right) Feature extraction.

2.3.4 Region Growing Algorithm Based Method

According to Lv *et al.*, 2017, the workflow of this method is shown in figure 2.15. First, a robust semi-supervised fuzzy C-means (RSFCM) clustering algorithm is adopted to generate the change magnitude image (CMI) from bi-temporal images (Shao *et al.*, 2016). However, images in different timestamps

for change detection are usually different in radiation due to different sun angles, soil moisture and atmospheric conditions. Thus, the result of the image difference will become unreliable.

After that, an automatic noise reduction algorithm based on OTSU's method and Gaussian filter (GF) is employed to further filter the noise in CMI. OTSU's method is a method used to perform automatic image thresholding (Greensted, 2010). The GF has a drawback. It requires prior knowledge about the magnitude of the noise level. Figure 2.16 shows the flowchart of the discussed method.

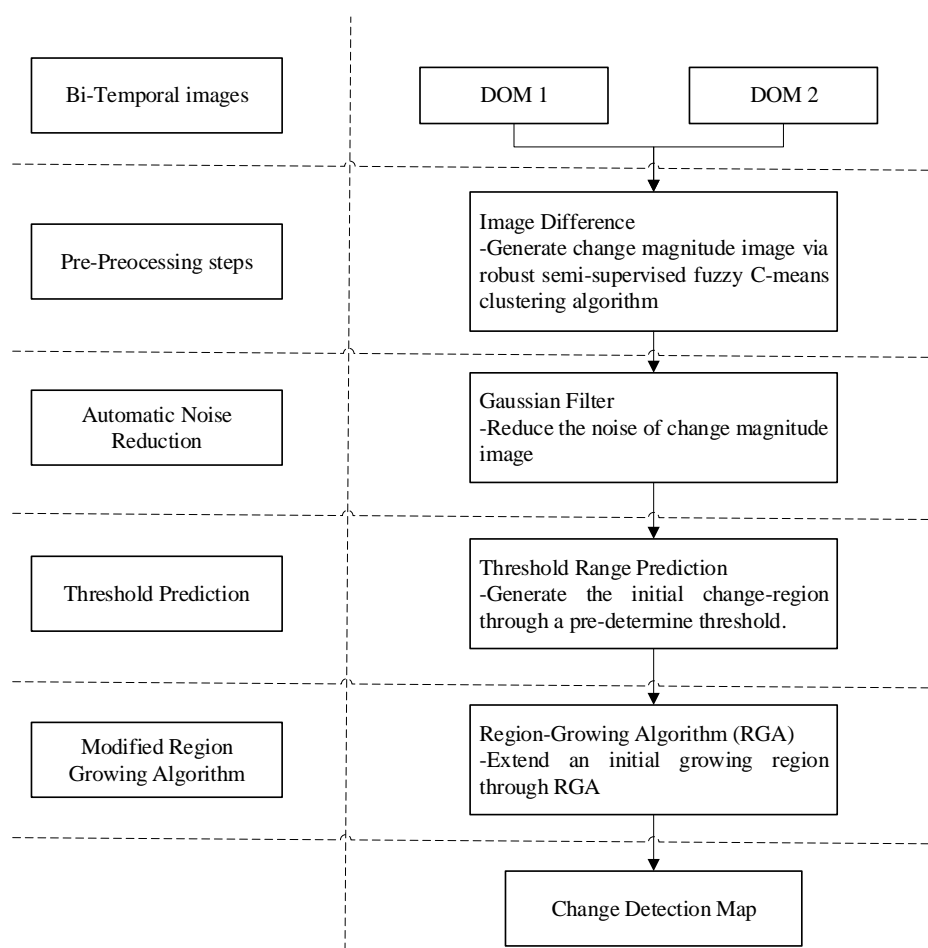


Figure 2.15: Processing Chain of Region Growing Algorithm Based Method.

The Gaussian filter radius (r) is adjusted via a continuous step, which takes the relationship between the OTSU-binary result and filtered image into account. The r is steadily increased from small to big. The filtered image is split into a binary image via OTSU. When the previously predicted binary threshold

(T) is equal to the current T , the current r can be considered as the optimised filtered radius.

After obtaining the filtered change magnitude image (FCMI), the FCMI will be converted into a binary change detection map (BCDM) through a thresholding process. However, setting a threshold to divide the CMI into BCDM is experience-dependent and tedious (Gong et al., 2014). Therefore, an automated threshold range prediction is carried out. The flowchart of the prediction is illustrated in figure 2.17. The pixels of FCMI can be separated into three categories, changed pixels, uncertain pixels and unchanged pixels. The difference between the three categories is uncertain and fuzzy.

First, histogram-based curve fitting is carried out at the FCMI. A moving least squares (MLS) is used as the method for curve fitting to smoothen the noise and correctly interpret the distributed patterns (Levin, 1998). Lastly, the curve fitting line's slope value is determined, and the threshold range can be captured.

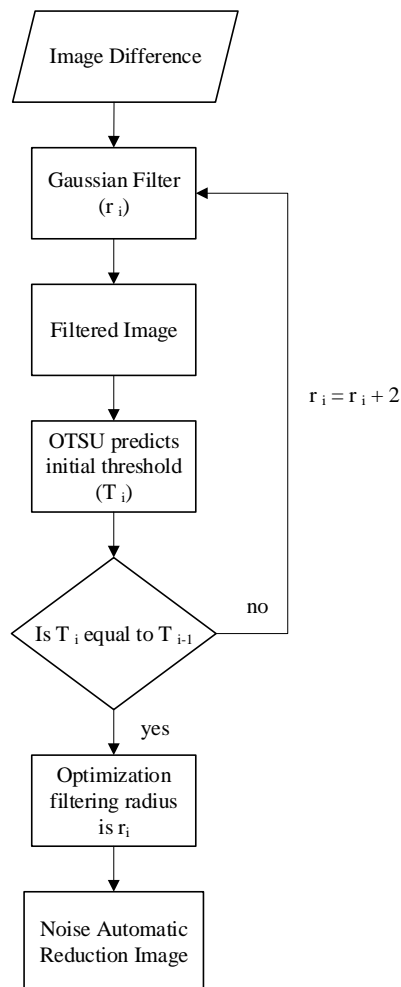


Figure 2.16: Steps of Automatic Noise Reduction Method.

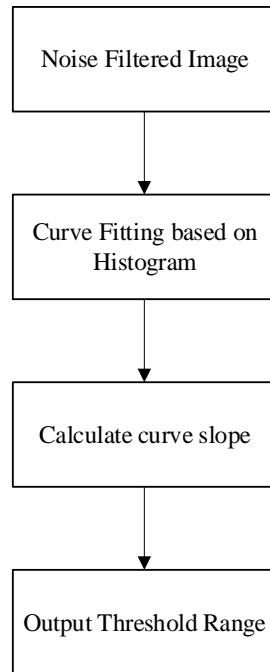


Figure 2.17: Steps of Threshold Range Prediction (TRP).

In this stage, the BCDM is generated. A modified regional growing algorithm (mRGA) is used to improve the result. In BCDM, the pixels of spatial change form a changing area called the initial growing region (IGR). The BCDM and FCMI are superimposed together, and the FCMI pixels within the IGR are used to construct a corresponding credible interval (CI). The seed pixel, pixels on the edge of ICR will grow until no pixel can be found (Lv *et al.*, 2017). The mRGA process is shown in figure 2.18 to clarify the growing procedure.

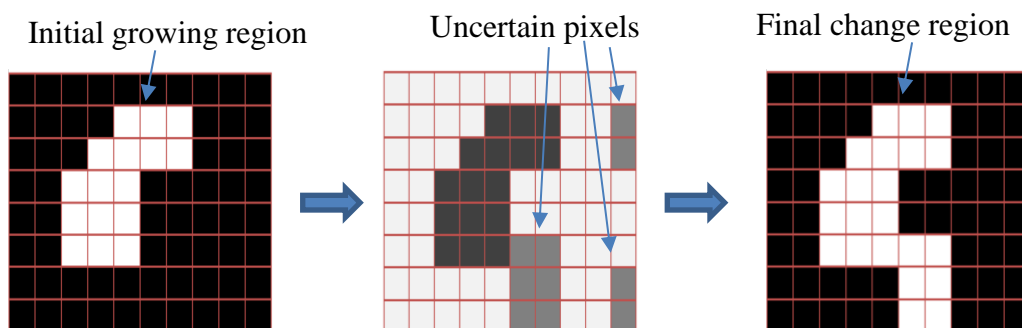


Figure 2.18: Illustration of mRGA.

2.3.5 PCA and K-means Clustering Method

According to Celik, 2009, the workflow of this method is shown in figure 2.19. It is a type of unsupervised change detection in multitemporal satellite images using PCA and K-means clustering. First, two images from different timestamps are used to create a “difference image”. After that, the difference image is partitioned into h times h non-overlapping blocks followed by eigenvector extraction through PCA. Then, project the difference image h times h neighbourhood data onto the eigenvector space to create the feature vector for each pixel. Then, carry out the K-means clustering to generate two clusters from the feature vector space. Lastly, based on the Euclidean distance between the feature vector and the clusters mean feature vector, assign each pixel of the difference image to one of the clusters. The cluster whose pixels have a higher average value in the difference image is assigned as the changes class, and the other cluster is assigned as the non-changes class.

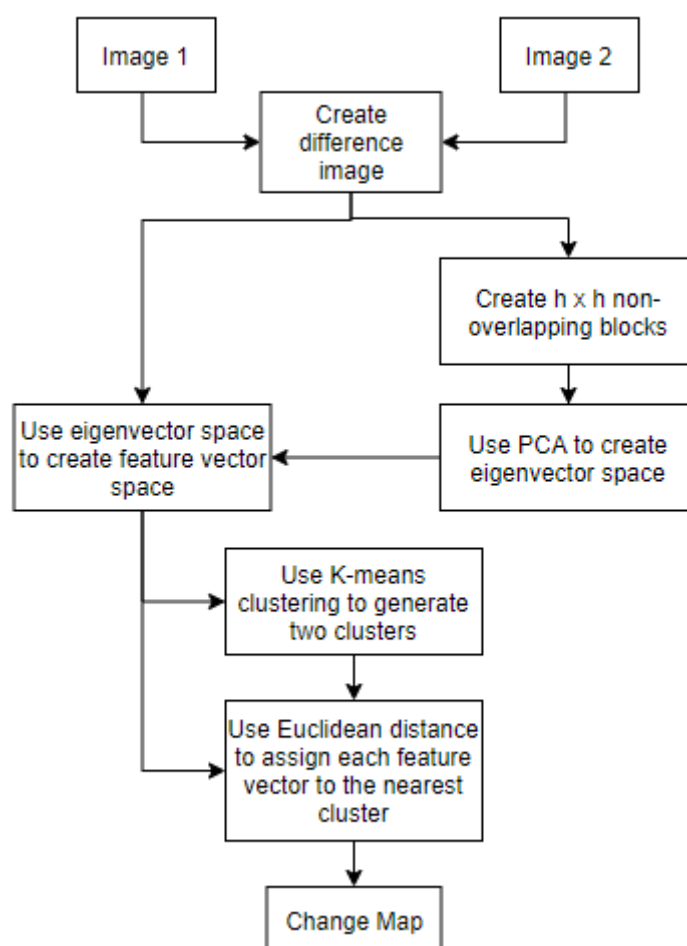


Figure 2.19: Workflow of PCA and K-means Clustering Method.

The author compared its method with two other methods: expectation-maximisation (EM)-based thresholding and Markov random fields (MRF)-based thresholding presented by Bruzzone and Prieto, 2000. The result of the comparison is shown in figure 2.20 and figure 2.21. PSNR stands for peak signal-to-noise ratio between images. The lower the PSNR, the more the noises.

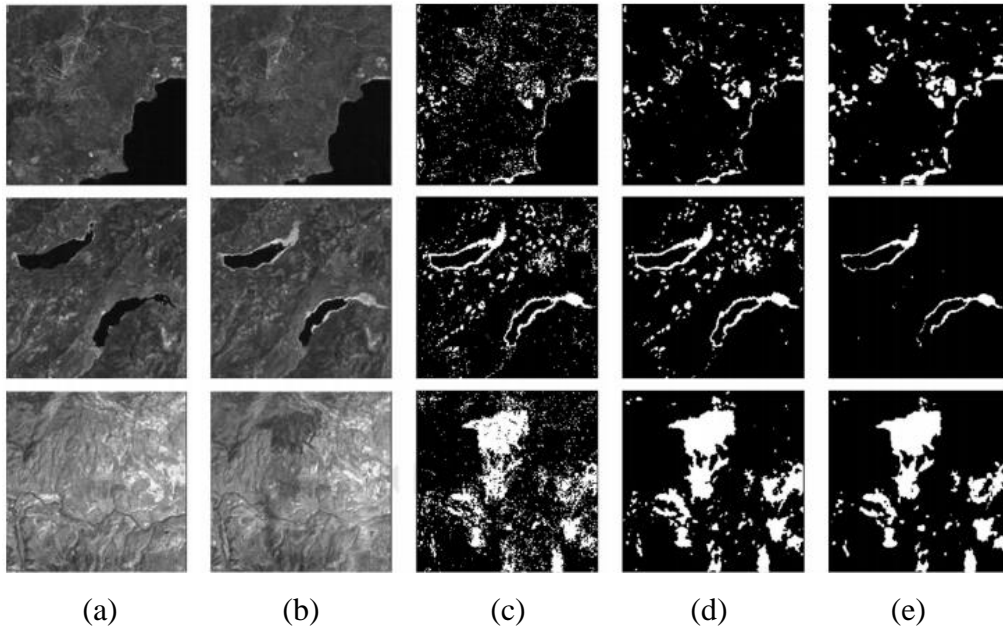


Figure 2.20: Comparison of Change Detection Results (Celik, 2009). (a) Input image 1. (b) Input image 2. (c) EM-based. (d) MRF-based. (e) PCA K-means Clustering.

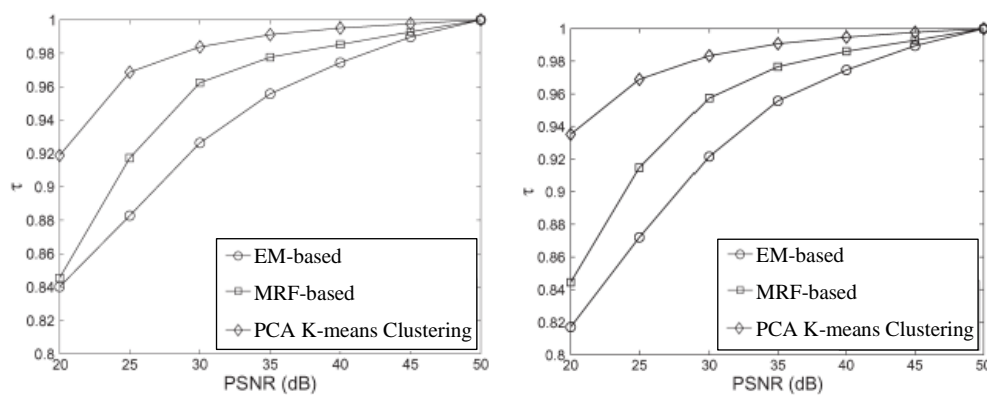


Figure 2.21: Detection performance comparisons against different levels of noises (Celik, 2009). (Left) Speckle noise. (Right) Zero-mean Gaussian Noise.

According to the results, PCA K-means Clustering performs better against noise. As shown in figure 2.21, the PCA K-means clustering is clearly

more robust against various forms of noise. The method is relatively stable against the speckle noises and zero-mean Gaussian, where the maximum rate of change is 8 % for speckle noise and 6 % for zero-mean Gaussian noise with respect to zero noise change detection performance. This demonstrates the superiority of the PCA K-means clustering.

The change detection of DOM generated from the drone's aerial footage is very similar to satellite images. They both faced the issue of weather conditions, sun light position, noises from trees and other random errors. The noises of DOM will be much larger than satellite images due to the reconstruction process. It is almost impossible to reconstruct a tree perfectly. This project's area of interest is a rural area mainly covered by trees and green vegetation. Thus, the method that can create a good result when facing noises is the main priority. Finally, the PCA K-means clustering method is selected as the backbone of the methodology for change detection with the help of the idea of the region growing algorithm based method.

CHAPTER 3

METHODOLOGY AND WORK PLAN

3.1 Project Flow

The project flow can be separated into three parts, mapping process, 2D and 3D map reconstruction, and change detection. The flow chart of the project is shown in figure 3.1. The yellow boxes are the objectives of this project.

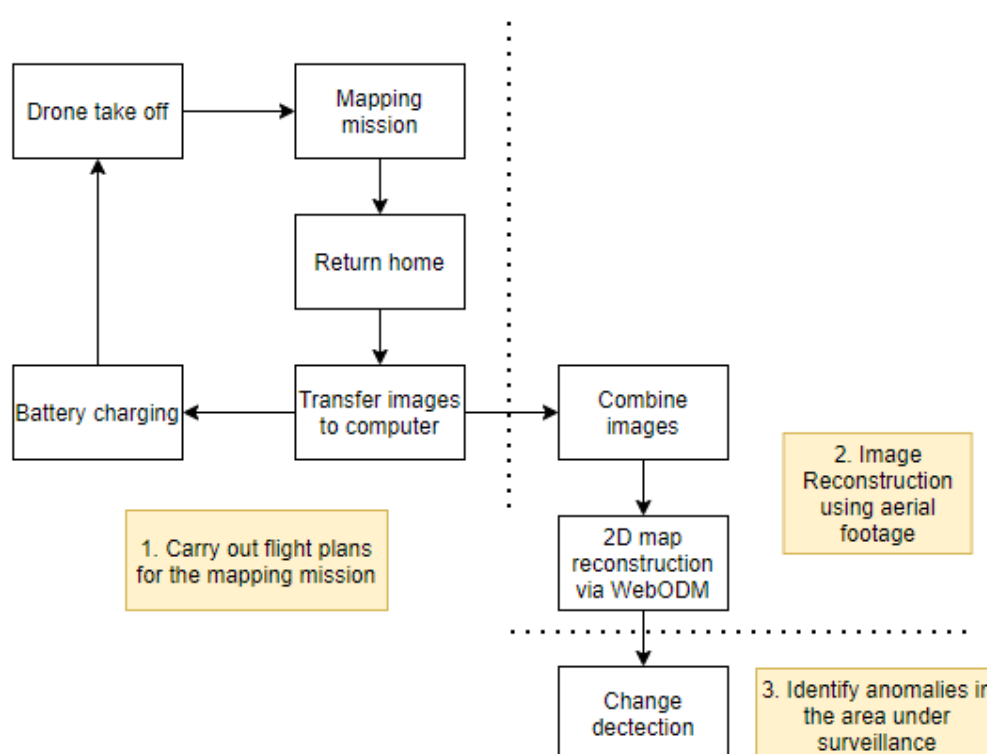


Figure 3.1: Project Flow Chart.

As mentioned in section 2.1.3, “DJI Mavic 2 Enterprise Dual” is selected. The drone is shown in figure 3.2. The specifications of the drone are listed in Appendix A. The drone will map the area of interest via a phone application called “DJI Pilot”. The mapping mission is basically a drone flying according to the flight plan and capturing images along the way. In “DJI Pilot”, the area of interest can be marked down by the user, as shown in figure 3.3. This map can be saved, and it is called a flight plan. In the “DJI Pilot”, some parameters can be tuned, such as side overlap ratio, frontal overlap ratio, margin, altitude,

and others. Once the command is given to the drone, the drone will take off from the control centre and autonomously start the mapping process.



Figure 3.2: DJI Mavic 2 Enterprise Dual.

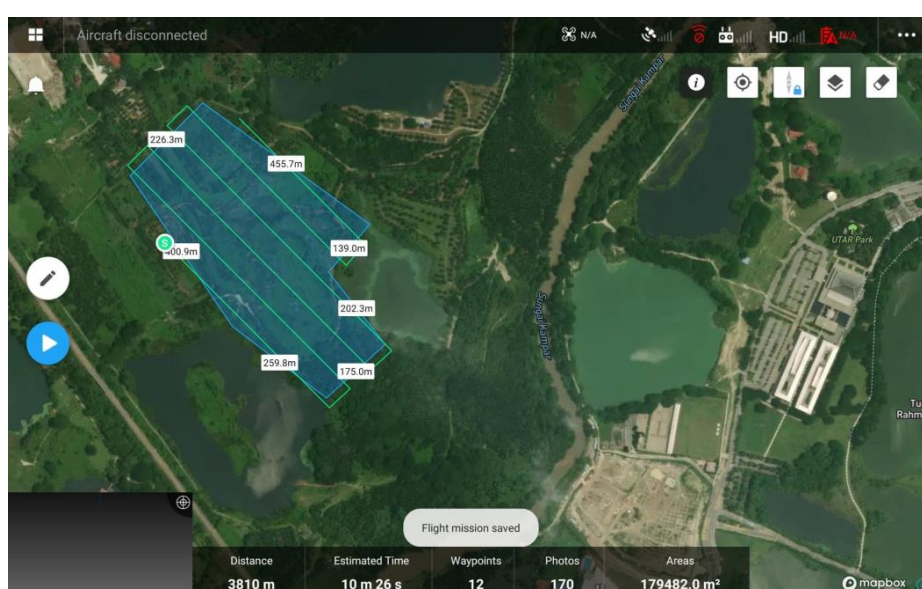
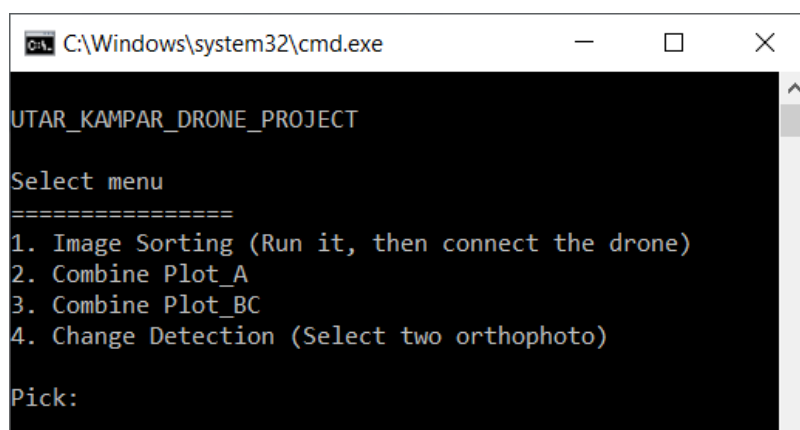


Figure 3.3: Mapping Mission by using DJI Pilot.

After completing the mapping mission, the drone will return to the control centre by itself without any human intervention. After that, the operator needs to run a batch file. Batch file is a script file which consists of a series of commands to be executed by the command-line interpreter. It is like a user interface to ease out the process of running the python script. A window will show up, as shown in figure 3.4. There are four choices that the user can select. Option number one is for transferring images from the drone into a computer and sorts them. Option number two and three is for combining the images from the same plot. After carrying out option number one to three, the images are needed to upload on to the WebODM. Once the reconstruction process is completed, option number four can be carried out. Option number four is for

change detection. Details of these selections and processes will be discussed later.



```

C:\Windows\system32\cmd.exe

UTAR_KAMPAR_DRONE_PROJECT

Select menu
=====
1. Image Sorting (Run it, then connect the drone)
2. Combine Plot_A
3. Combine Plot_BC
4. Change Detection (Select two orthophoto)

Pick:

```

Figure 3.4: Batch File with Two Options.

3.2 Mapping

The area needed to be under surveillance by drone is quite large. Therefore, the area had been divided into three main sections, plot A, plot B, and plot C. Figure 3.5 shows the lands owned by UTAR. The red solid line boundary is the land owned by UTAR. The black dotted line boundary is the area under the surveillance of this drone project. Plot A is further divided into five sections. Plot B is divided into two sections. Lastly, plot C is divided into four sections.

The separation of the plot is due to the battery life of the drone. The maximum flight time of the drone is 31 minutes when there is no wind. After consideration, the flight time of each section is around 10 minutes. Total of 11 flight trips are required to complete the mapping process. Plot A covers an area of around 918 023 m² (226.85 Acres). Plot B covers an area of around 255 521 m² (64.14 Acres). Plot C covers an area of around 797 526 m² (197.08 Acres). The flight missions of each plot are shown in Appendix B. The altitude of the drone is 100 m. The take-off speed is 10.3 m/s. The speed is 6.5 m/s. The ground sampling distance is 3.06 cm/pixel. It is the distance between the centres of two adjacent pixels. 3.06 cm/pixel means that one pixel on the aerial image represents 3.06 cm in the real world. In order to get the flight permission from the Civil Aviation Authority of Malaysia, the flight planning of the operation

area is drawn. Same as the flight mission, there are 11 of them which are constructed on the google map as shown in Appendix C.

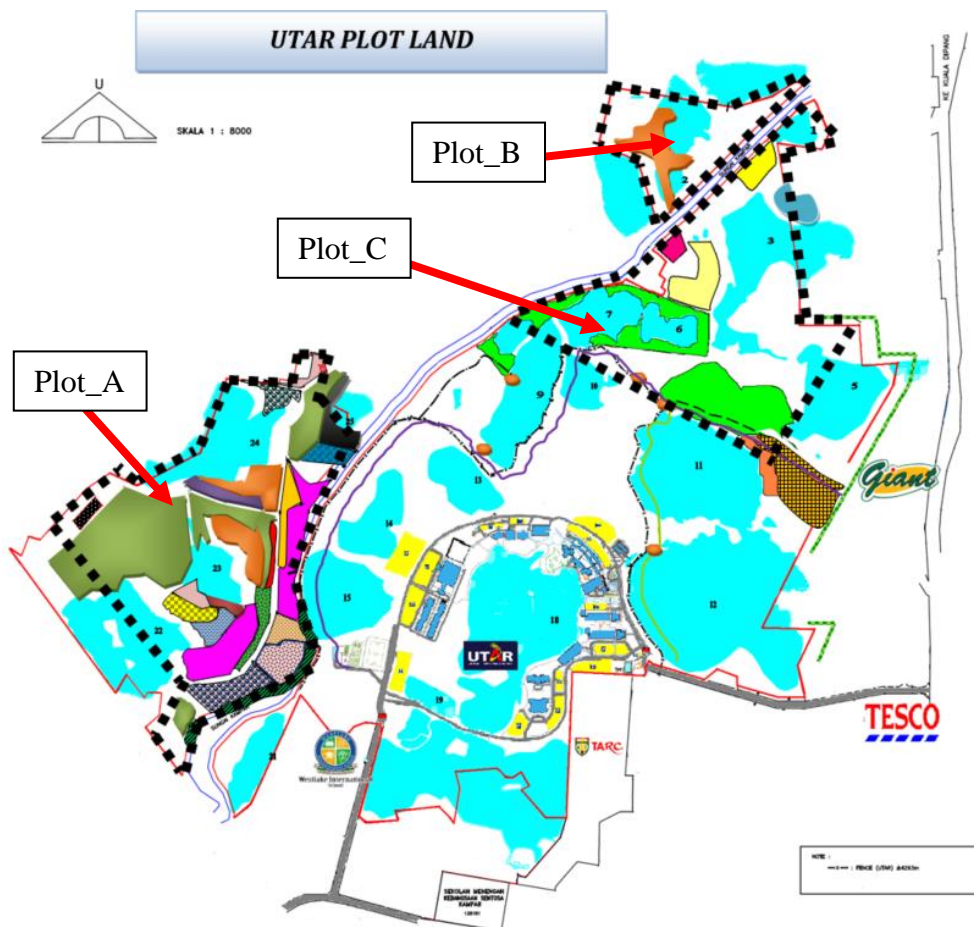
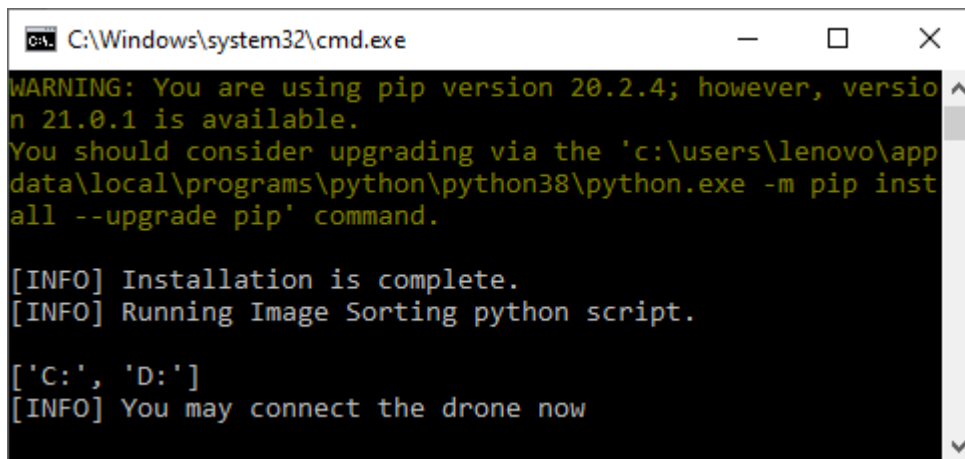


Figure 3.5: Lands Owned by UTAR.

3.3 Sort and Transfer Images

The sorting of the aerial images can be divided into two parts. Option number one, and option number two and three in figure 3.4. Once the user has chosen option one, the batch file will download all the libraries required for the image sorting python script. Once the installation is completed, it will ask the user to connect the computer and the drone, as shown in figure 3.6.



```

C:\Windows\system32\cmd.exe
WARNING: You are using pip version 20.2.4; however, version 21.0.1 is available.
You should consider upgrading via the 'c:\users\lenovo\appdata\local\programs\python\python38\python.exe -m pip install --upgrade pip' command.

[INFO] Installation is complete.
[INFO] Running Image Sorting python script.

['C:', 'D:']
[INFO] You may connect the drone now

```

Figure 3.6: After Select Option One.

After connecting the drone to the computer through a USB cable, the script will detect it and transfer the images from the drone to the computer autonomously. This process needs to be carried out immediately after the drone completes one flight mission. Mixed aerial images are not allowed because the sorting is based on coordinate. If the aerial images are mixed, the software will be unable to sort the images correctly. The program will read the date taken and coordinate of every single image in the drone. The program will further move the images into their respective folder based on the mean of the coordinates. A tolerance of 0.0005 is given, which is around 55 m. The mean of the coordinates for each plot is shown in figure 3.7. Besides, the program will separate the IR images and the RGB images based on their size. IR images are much smaller than RGB images. The directory is shown below.

```

+----Plot_A_1
|   \---Flight_1_Jan 25 2021
|       +----ir_camera
|           |
|           +----main_camera
|               |
|               \---webodm_output

```

```

PLOT = {
  "Plot_A_1": ["4.345484072937968", "101.13208895671437"],
  "Plot_A_2": ["4.342515417478882", "101.1296573079922"],
  "Plot_A_3": ["4.341026848989899", "101.126195666835"],
  "Plot_A_4": ["4.33823593192036", "101.13026492790623"],
  "Plot_A_5": ["4.335555188164251", "101.12813330338166"],

  "Plot_B_1": ["4.356269368098159", "101.14496708111794"],
  "Plot_B_2": ["4.357318080737278", "101.14831750259607"],

  "Plot_C_1": ["4.351184531504065", "101.14460775508131"],
  "Plot_C_2": ["4.353780342333954", "101.14858688175048"],
  "Plot_C_3": ["4.347414316190476", "101.14688937079364"],
  "Plot_C_4": ["4.349559705065359", "101.14958367238563"],
}

```

Figure 3.7: Mean of Coordinates for Each Plot.

After completion of every flight mission, it is the turn of option two and three. Option two will combine every image in Plot_A_1, Plot_A_2, Plot_A_3, Plot_A_4, and Plot_A_5. Option three will combine every image in Plot_B_1, Plot_B_2, Plot_C_1, Plot_C_2, Plot_C_3, and Plot_C_4. It will combine them based on the flight number. Figure 3.8 shows the process run by the program after select option 2.

```

C:\Windows\system32\cmd.exe
4. Change Detection (Select two orthophoto)
Pick:2
[INFO] Running Selection Num Two (Combine Plot_A)
[INFO] Running Combine Plot_A python script.
[INFO] The latest flight in the folder is equal: Flight 1
[INFO] Start to combine all Plot_A.
[INFO] New folder created: D:\UTAR_Kampar\Plot_A\Flight_1\images
[INFO] Please wait, copying Plot_A_1
[INFO] Please wait, copying Plot_A_2
[INFO] Please wait, copying Plot_A_3
[INFO] Please wait, copying Plot_A_4
[INFO] Please wait, copying Plot_A_5
[INFO] Completed combine Plot_A. Total of 785 images.
Press any key to continue . . .

```

Figure 3.8: Option Two.

3.4 WebODM

Once the combination is completed, the reconstruction process will be run by a software called WebODM. WebODM is actually identical to ODM, just that it has a user-friendly interface. The data and projects can be organised more quickly in the WebODM. Figure 3.13 shows the dashboard of the WebODM. The method of the WebODM to reconstruct the 2D and 3D map is stated in section 2.2.

The WebODM had been set up in the UTAR server. The user can access it through <http://rsc.utar.edu.my:8500/>. The steps to carry out the reconstruction process are stated below.

1. Click “Select Images and GCP”. (Figure 3.9)
2. Select images and press “Open”. (Figure 3.10)
3. Name the task accordingly. (Figure 3.11)
4. Choose the option “UTAR_Kampar”. (Figure 3.11)
5. Click “Preview”. (Figure 3.11)
6. Click “Start Processing”. (Figure 3.12)
7. Leave the webpage until the uploading process is completed. (Figure 3.13)
8. Download the orthophoto.

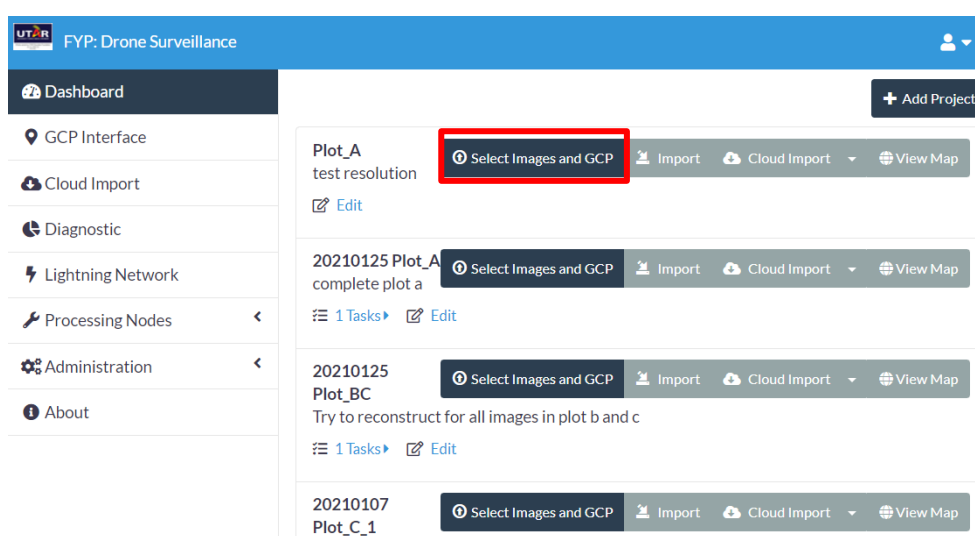


Figure 3.9: Click “Select Images and GCP” to upload images.

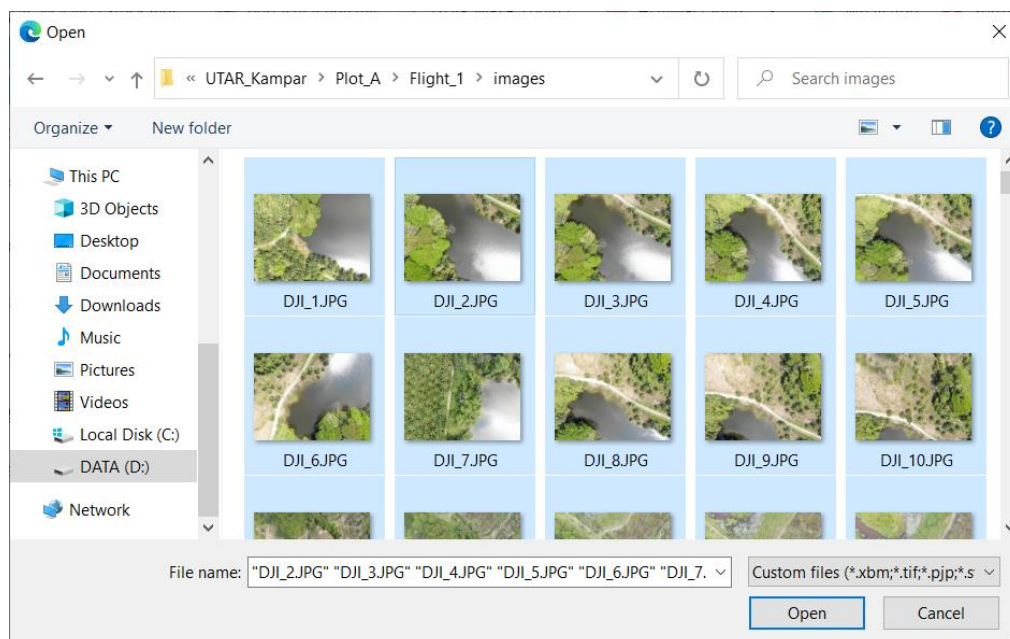


Figure 3.10: Select images and press “Open”.

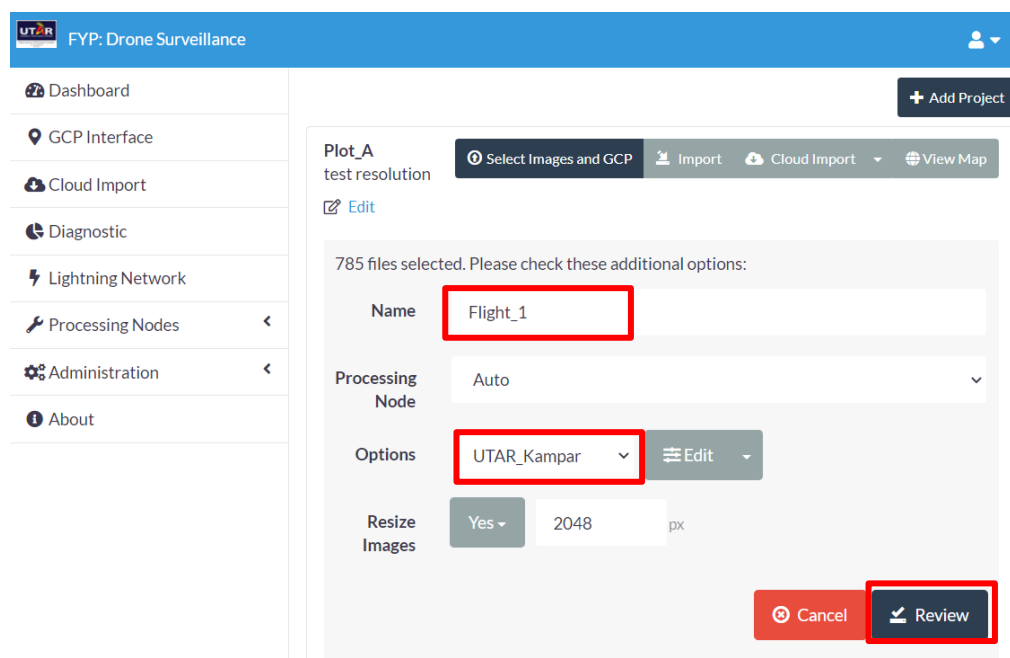


Figure 3.11: Name the tasks accordingly, choose option “UTAR_Kampar” and click “Preview”.

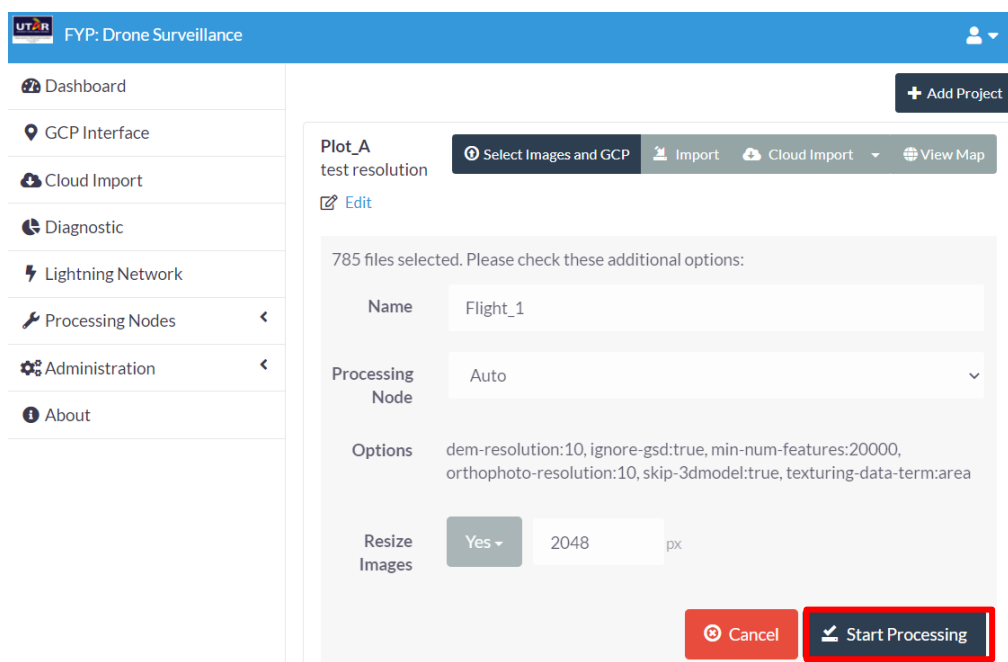


Figure 3.12: Click “Start Processing”.

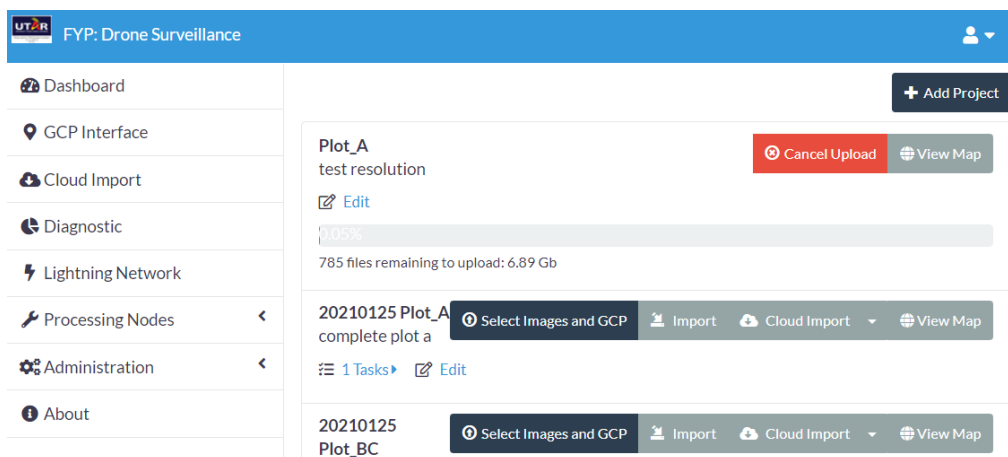


Figure 3.13: Leave the webpage open until the uploading process is completed.

In step number four, choose option “UTAR_Kampar”. It is a special option built for this project. This option includes `ignore-gsd: true`, `dem-resolution: 15`, `orthophoto-resolution: 15`, `min-num-features: 20000`, `skip-3dmodel: true`, `texturing-data-term: area`.

3.4.1 Ignore-gsd

Ground Sampling Distance (GSD) is for the system to achieve good processing speed. In default, GSD caps the maximum resolution of orthophotos and resizes

images when necessary. In this project, a constant orthophoto-resolution is needed. Therefore, the option `ignore-gsd` has been enabled.

3.4.2 Dem-resolution

This option specifies the output resolution of DEMs in cm/pixel. As an example, if the area covered by the point cloud is 100 x 50 meters and dem-resolution is set to 10 cm/pixel, the final image size of the DEM in pixels can be calculated by:

$$\frac{(100 \text{ m} \times 100 \frac{\text{cm}}{\text{m}})}{10 \text{ cm/pixel}} = 1000 \text{ pixels}$$

$$\frac{(50 \text{ m} \times 100 \frac{\text{cm}}{\text{m}})}{10 \text{ cm/pixel}} = 500 \text{ pixels}$$

So, the output DEM will be an image of 1000 x 500 pixels.

3.4.3 Orthophoto-resolution

It is the same as dem-resolution but applied to orthophotos instead of DEMs. The unit is in cm/pixel.

3.4.4 Min-num-features

During the SFM process, images have to be matched into pairs. The way the pairing happens is by means of finding matches between features in the images. If the same feature is found to be present between two images, it is used as evidence of a possible match. This option controls the minimum number of features the program tries to find in each image, thus increasing the likelihood of finding matches between images. In this project, the area of interest is a rural area with many trees and green vegetation. These areas have few distinguishable features. Therefore, the min-num-features should be increased to increase the chances of a match between images. It could also help to generate a complete orthophoto.

3.4.5 Skip-3dmodel

This option saves some time by skipping the commands that produce a 3D model. The 2.5D model is a model where elevation is directly extruded from the

ground plane. It is not a true 3D model but works well for the purpose of rendering orthophotos.

3.4.6 Texturing-data-term

The difficult part of texturing a mesh is answering the question of how to choose the best image for each part of the mesh. Since due to overlap, each part of the mesh has likely been photographed by multiple images. This process is known as view selection and is guided by the definition of a data term. There are two data terms available, Gradient Magnitude Image (GMI) and area. Area is chosen instead of GMI due to the tree having a high gradient magnitude. If GMI is used, a higher likelihood of inconsistent texture may happen.

3.5 Change Detection

After completing the reconstruction and obtaining the DOM, change detection can be carried out by selecting option number four in the batch file, which had been shown in figure 3.4. Like option one, the batch file will download all the libraries required for the change detection python script. Once the installation is complete, a user interface will pop out, as shown in figure 3.14 and ask the user to choose two orthophotos for change detection.

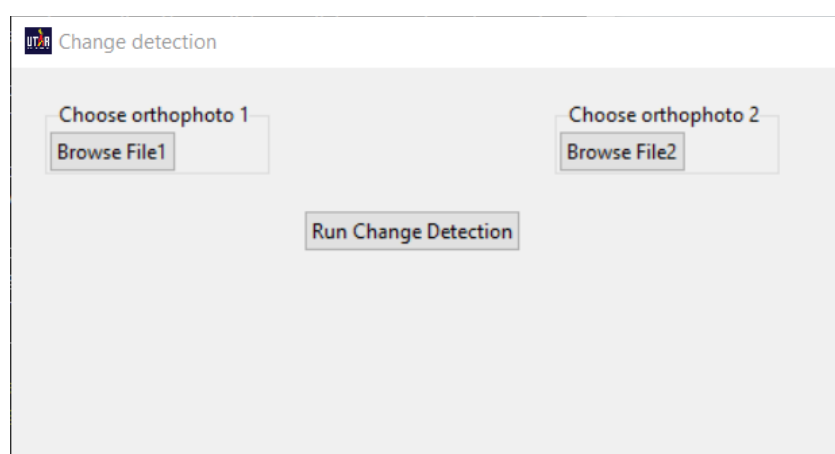


Figure 3.14: User Interface for Change Detection.

The change detection is purely based on DOM. DSM and digital terrain model (DTM) are not taken into consideration due to the quality of the 3D model result. The user interface is shown in figure 3.15. Orthophotos can be selected

through “Browse File” which is highlighted by red boxes. The “Run Change Detection” at the bottom of the centre is to start the change detection process. The process of change detection is shown in the figure 3.16.



Figure 3.15: User Interface of Change Detection After Selected Two Images.

3.5.1 Realign Orthophoto

The boundary of the DOM created will always be different. Therefore, the realignment of DOM is needed before carrying out the change detection. The realignment is also known as image registration. The alignment of DOM is achieved by using coordinate as reference. DOM is georeferenced, meaning that the image has been tied to a known earth coordinate system.

The boundary coordinate of two different DOMs will be read. Based on the boundary, a new boundary will be created, as shown in figure 3.17. The blue box is the boundary of DOM_1. The green box is the boundary of DOM_2. A new boundary, red dotted line box will be created. The DOM_1 and DOM_2 will be put into this common boundary.

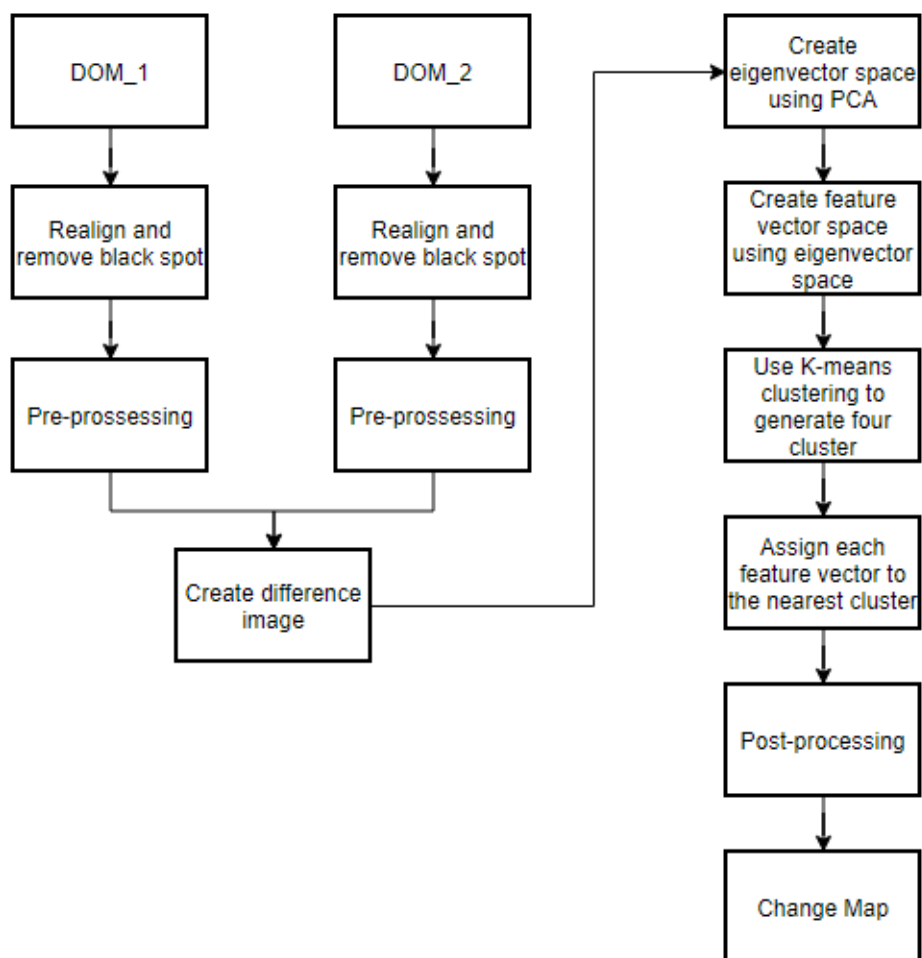


Figure 3.16: Flow Chart of Change Detection.

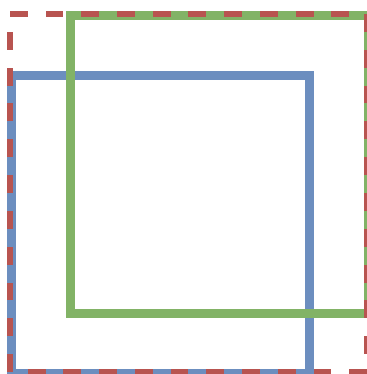


Figure 3.17: Illustration of the Realignment of DOM.

3.5.2 Remove Black Spot

After realignment, another process called remove black spot will be carried out. Figure 3.18 shows the original DOM. The DOM shape is irregular. Thus, the area which failed to reconstruct in either DOM will be removed.

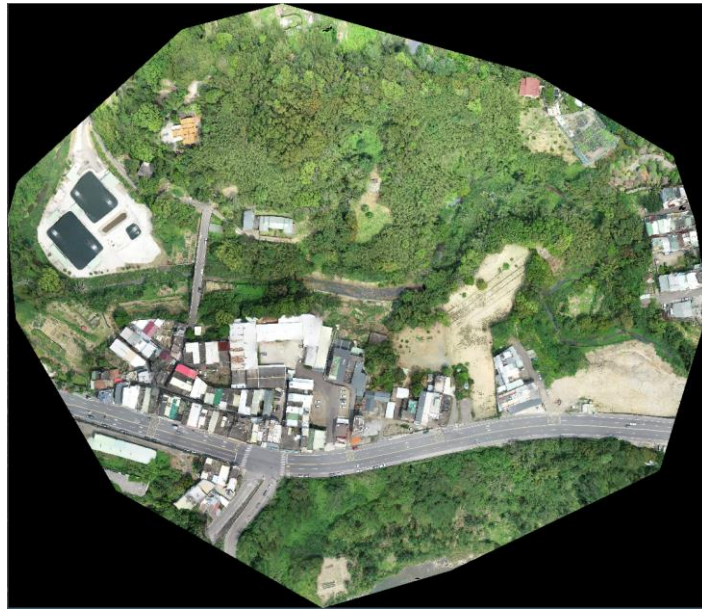


Figure 3.18: DOM Before Realignment.



Figure 3.19: DOM After Realignment.

3.5.3 Pre-processing

Before change detection, the DOM will go through histogram equalisation followed by gaussian blur. This is to minimise the effect of sunlight during the mapping process. Figure 3.20 shows the DOM after the preprocessing process.

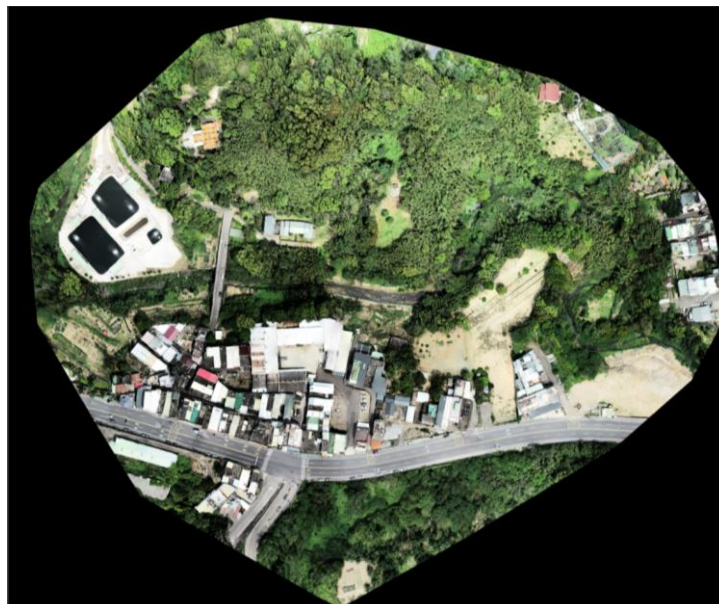


Figure 3.20: DOM After Pre-processing.

3.5.4 Image 1 – Image 2

Figure 3.21 shows the absolute difference between DOM_1 and DOM_2.

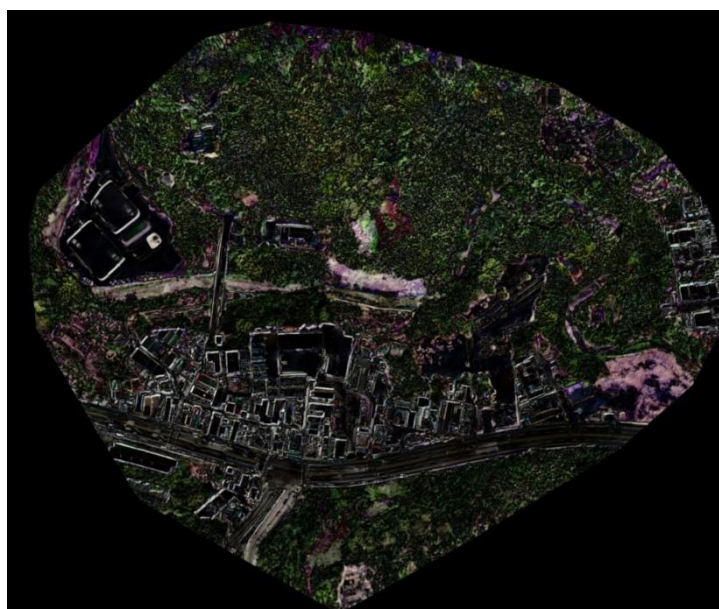


Figure 3.21: Difference Image.

3.5.5 PCA and K-Means Clustering

PCA stands for principal component analysis. PCA is used to extract the eigenvectors. A feature vector is extracted for each pixel of the difference image by projecting its neighbourhood data onto eigenvector space. After that, using the k-means algorithm to cluster the feature vector space into four clusters. Each

cluster is represented with a mean feature vector. Lastly, change detection is accomplished by assigning each pixel of the difference image to one of the clusters based on the shortest Euclidean distance between its feature vector and the mean feature vector of the clusters. The cluster whose pixels have the highest average value will be the change map. The binary change map is shown in figure 3.22, in which “white” indicates that the corresponding pixel location involves changes, whereas “black” involves no changes.

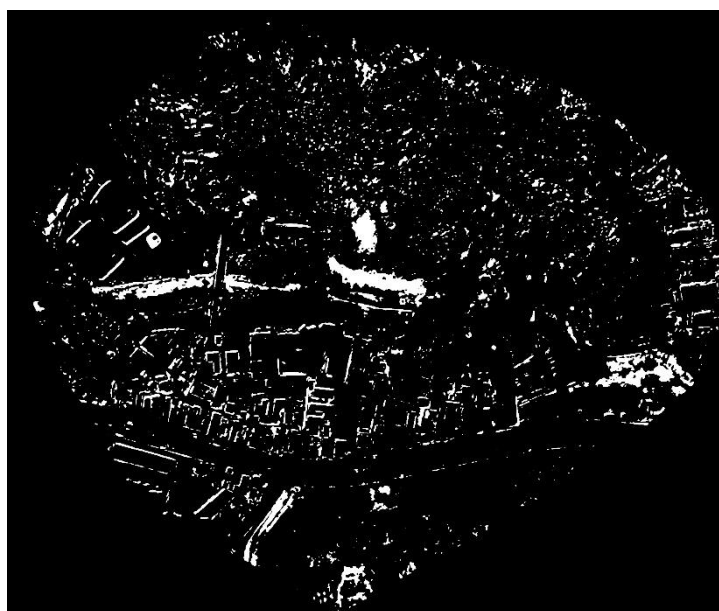


Figure 3.22: Binary Change Map.

3.5.6 Post-processing

The post-processing is to minimise the false-positive error. The reconstruction of DOM is not perfect. Some artefacts or miss alignment will be counted as changes. These false errors can be removed via morphology. The change map will go through opening morphology followed by closing morphology. Opening is just erosion followed by dilation. Most of the noises can be removed, as shown in figure 3.23. Figure 3.24 and figure 3.25 shows the orthophotos with highlighted changes.

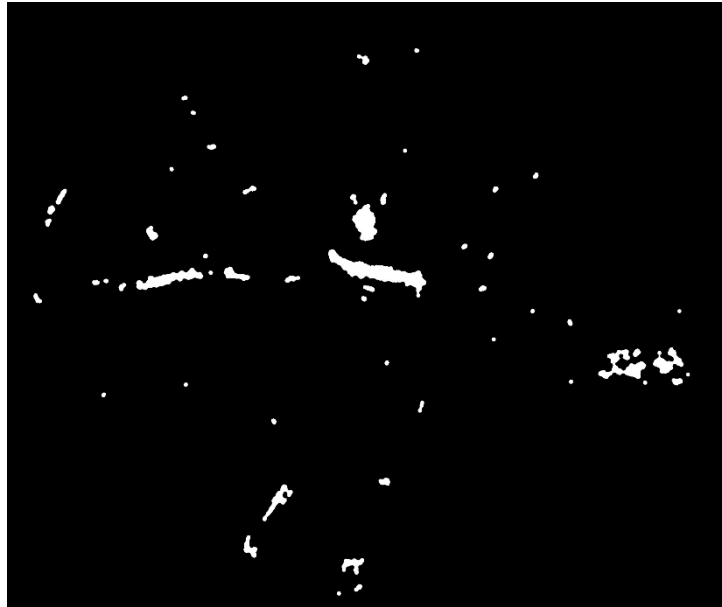


Figure 3.23: Change Map After Post-processing.

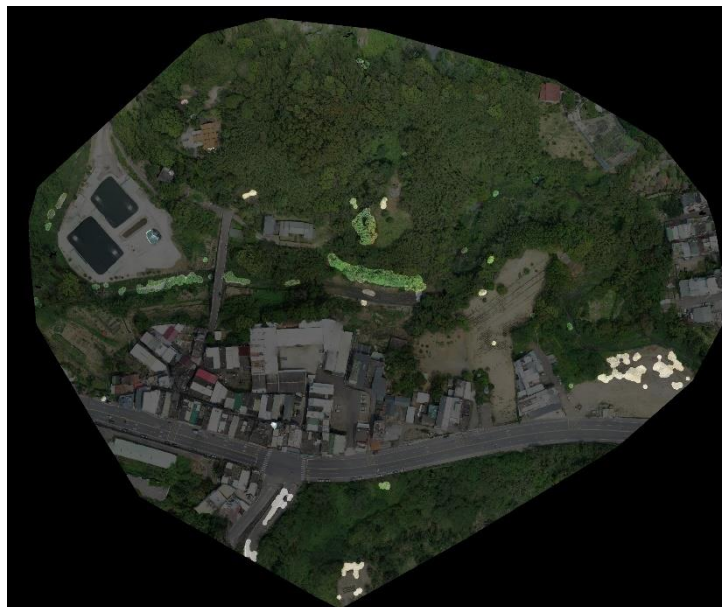


Figure 3.24: Orthophoto 1 with Highlighted Changes.

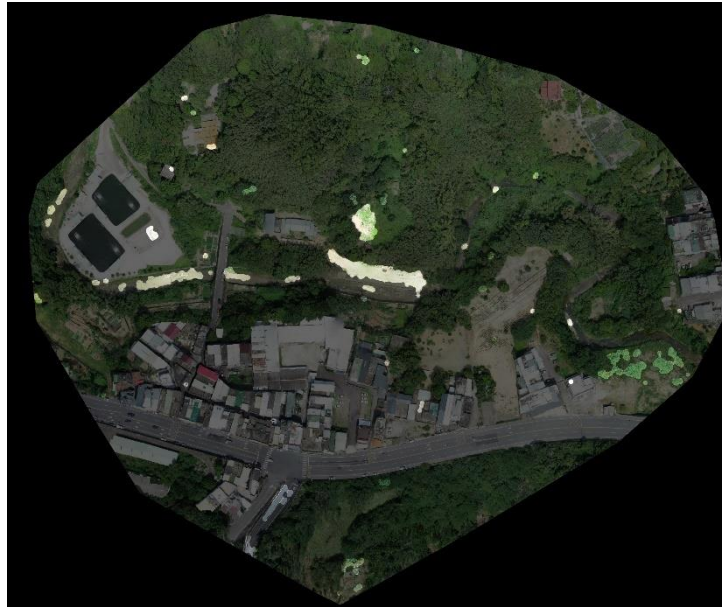


Figure 3.25: Orthophoto 2 with Highlighted Changes.

CHAPTER 4

RESULTS AND DISCUSSIONS

4.1 WebODM Results

In this section, the results of WebODM will be discussed. WebODM will reconstruct the orthophoto. A dataset captured by the DJI Mavic 2 enterprise is used for reconstruction. The mapping is set in a rural area in Kuala Selangor. This is to mimic the condition of the UTAR Kampar area.



Figure 4.1: Flight Map of the Kuala Selangor Rural Area.

4.1.1 Parameters

In this section, the effect of the parameters on the orthophoto will be shown. The main objective of WebODM is to create orthophoto for change detection. The orthophoto needs to be complete with good quality. Several parameters of WebODM had been discussed in section 3.4. In this section, their effect will be shown. Few options in the WebODM are tested, including default, high resolution, and forest. The results are shown below. The background is from the Google satellite image.

The parameters for default are all in default.



Figure 4.2: Default Orthophoto.

The parameters for high resolution are ignore-gsd: true, dsm: true, depthmap-resolution: 1000, dem-resolution: 2.0, and orthophoto-resolution:2.0.



Figure 4.3: High-Resolution Orthophoto.

The parameters for forest are min-num-features: 18000, texturing-data-term: area.



Figure 4.4: Forest Orthophoto.

The custom parameters for the UTAR Kampar area are dem-resolution: 15, ignore-gsd: true, min-num-features: 20000, orthophoto-resolution: 15, skip-3dmodel: true, texturing-data-term: area.



Figure 4.5: Custom Parameter Orthophoto for UTAR Kampar Area.

As shown in figures above, the custom parameters produce the best result. It successfully reconstructs the full mapping area.

4.1.2 Orthophotos and 3D Points Cloud

In this section, the orthophoto reconstruction of the interest area: UTAR Kampar will be shown. The option for reconstruction is the custom parameters. As mentioned in section 3.3: sort and transfer image, there are a total of two images set, Plot_A and Plot_BC. These images are taken at different times and dates, but they can still put together and reconstruct out a complete orthophoto. The results of orthophotos are shown in figure 4.6 and figure 4.7. The results of the 3D points cloud are shown in figure 4.8 and figure 4.9. The time taken to reconstruct the Plot_A orthophoto is 1 hour and 42 minutes; Plot_BC is 2 hours and 17 minutes. Plot_A consists of 785 images and Plot_BC consists of 956 images. Besides, 62 GB RAM is allocated to the WebODM for carrying out the reconstruction.



Figure 4.6: Plot_A Orthophoto.



Figure 4.7: Plot_BC Orthophoto.



Figure 4.8: Plot_A 3D Points Cloud.



Figure 4.9: Plot_BC 3D Points Cloud.

4.2 Change Detection Results

In this section, a dataset from the WebODM community is used to carry out the experiment of change detection with different numbers of clusters. The images are from a location in Toufen, Miaoli County, Taiwan. The timestamp is from 11th April 2019 and 16th September 2019. The orthophotos are shown in figure 4.10.

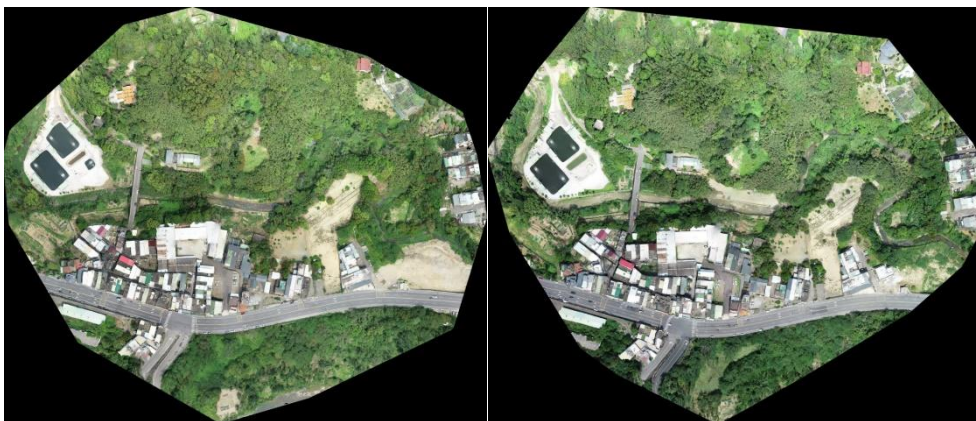


Figure 4.10: Orthophotos of Toufen, 11th Apr 2019 (Left) 16th Sept 2019 (Right).

After computing the change detection, the change maps produced by different numbers of clusters are obtained and shown in figures below. As mentioned in section 3.5.5, the feature vector space is clustered into several clusters using the k-means algorithm. The cluster whose pixels have the highest average value will be the change map. Therefore, the number of clusters will affect the final result a lot. When the number of clusters is two, there are a lot of noises as shown in figure 4.11. These noises are due to artifacts along the building edges and trees created during the reconstruction process. The algorithm will group these artifacts into the change map cluster.

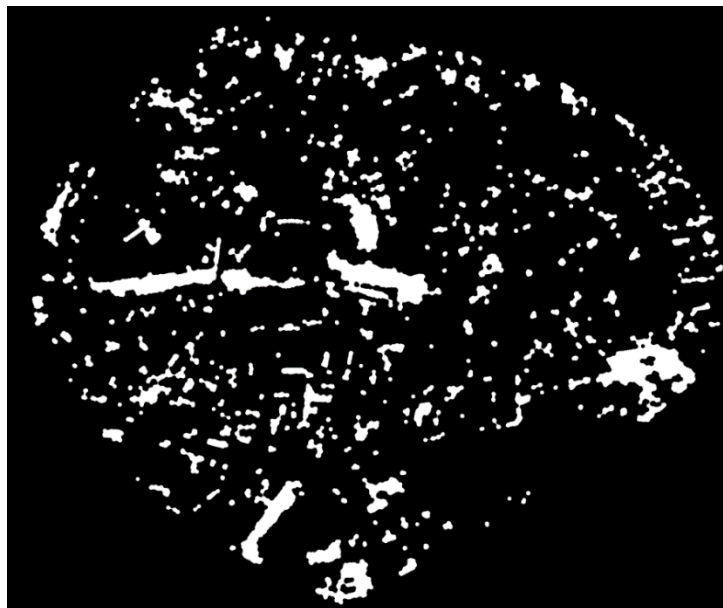


Figure 4.11: Change Map when the Number of Clusters is Two.

When the number of clusters is three, noises decrease as shown in figure 4.12. As the number of clusters increases, the algorithm starts to cluster the artifacts and noises as non-changes. For example, the first cluster is non-changes. The second cluster is for the artifacts and noises. The last cluster is for the true changes.

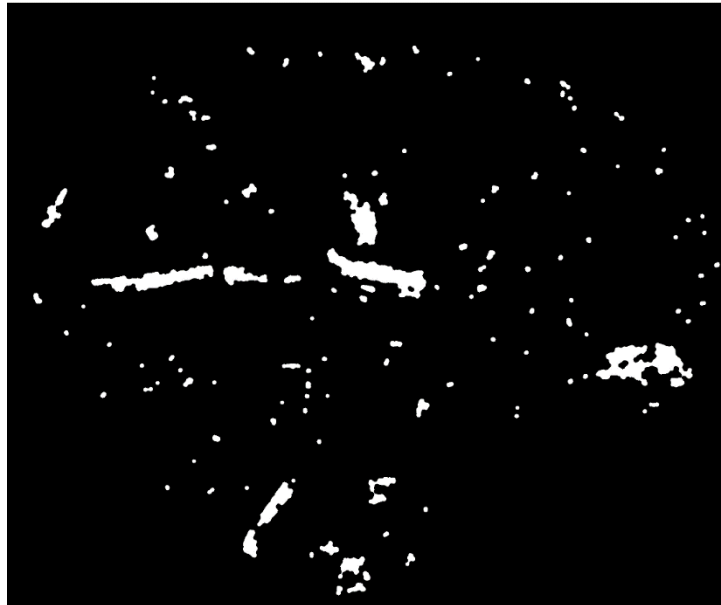


Figure 4.12: Change Map when the Number of Clusters is Three.

As shown in figure 4.13, When the number of clusters is four, almost only true changes remain. This is because only the pixels with a high value in the feature vector space will be counted as changes.

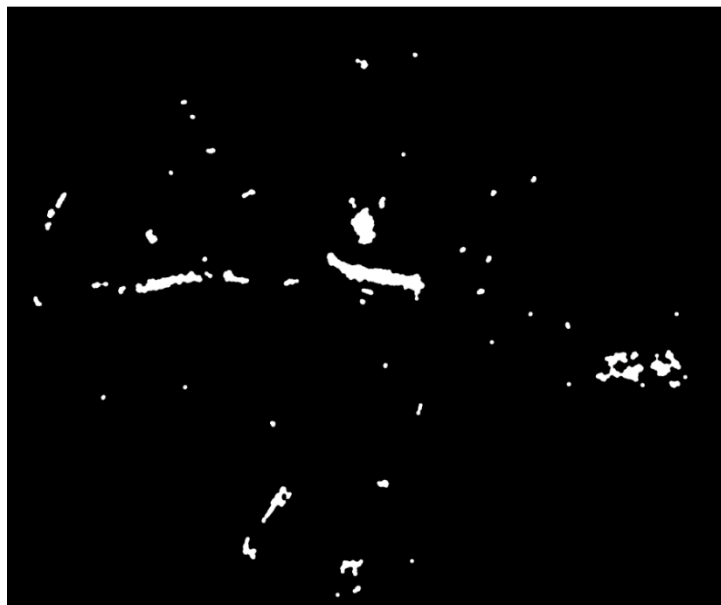


Figure 4.13: Change Map when the Number of Clusters is Four.

When the number of clusters is five, the result is the same as four as shown in figure 4.14. The additional cluster did not cause any difference to the change map.



Figure 4.14: Change Map when the Number of Clusters is Five.

As the number of clusters increases, the noise reduces gradually until the number of clusters is four. Figure 4.13 and figure 4.14 have shown they do not have any difference. It means that when the number of clusters is four, the changes and the non-changes have been clustered in their best form. Therefore, the final number of clusters is four. Figure 4.15 and figure 4.16 shows orthophoto 1 and 2 with highlighted changes.

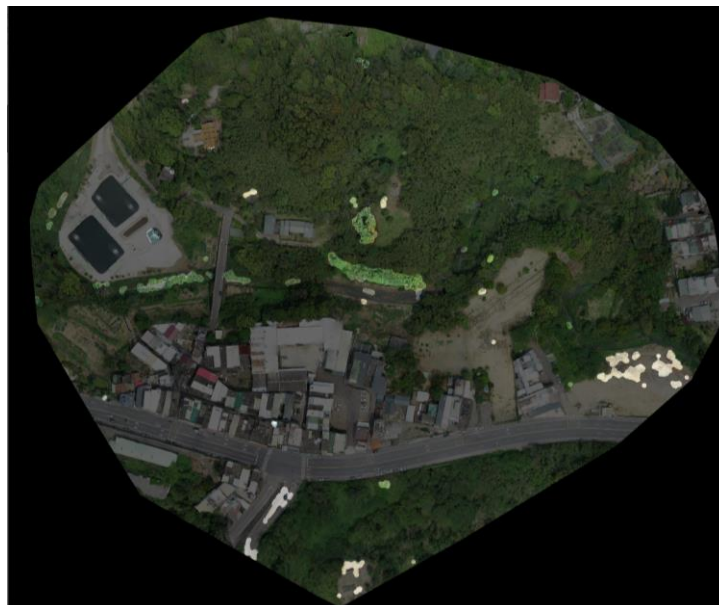


Figure 4.15: Orthophoto 1 with Highlighted Changes.

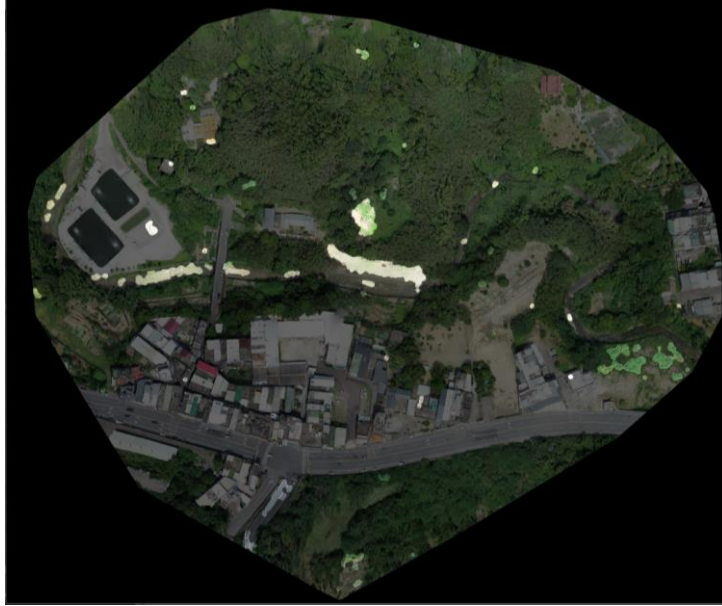


Figure 4.16: Orthophoto 2 with Highlighted Changes.

This algorithm also has its own weakness. Only orthophoto is used to detect changes, this caused the algorithm unable to detect changes which have a very similar RGB value as shown in figure 4.17. The building is a change, but only a small part of it is being detected.



Figure 4.17: Cropped Image from 11th April (Left) and 16th Sept (Right).

Besides, the change detection had also been carried out on the UTAR Kampar Plot_BC orthophoto. The two orthophotos used are actually from the same dataset. A different parameter is used for the reconstruction: texturing-data-term: gmi and min-num-features: 18000. These changes are to mimic the effect of orthophoto from two different timestamps. After that, the orthophoto is edited through a software called paint.net. Five changes are manually added

into the orthophoto. The final orthophoto is shown in figure 4.18 and the changes are circled by a red line. A small blue house is edited onto number one. Number two and three is a red house. Number 4 initially is full of green vegetation. Number five initially has land on it. The result of the change detection is shown in figure 4.19. All of the changes had been found successfully.

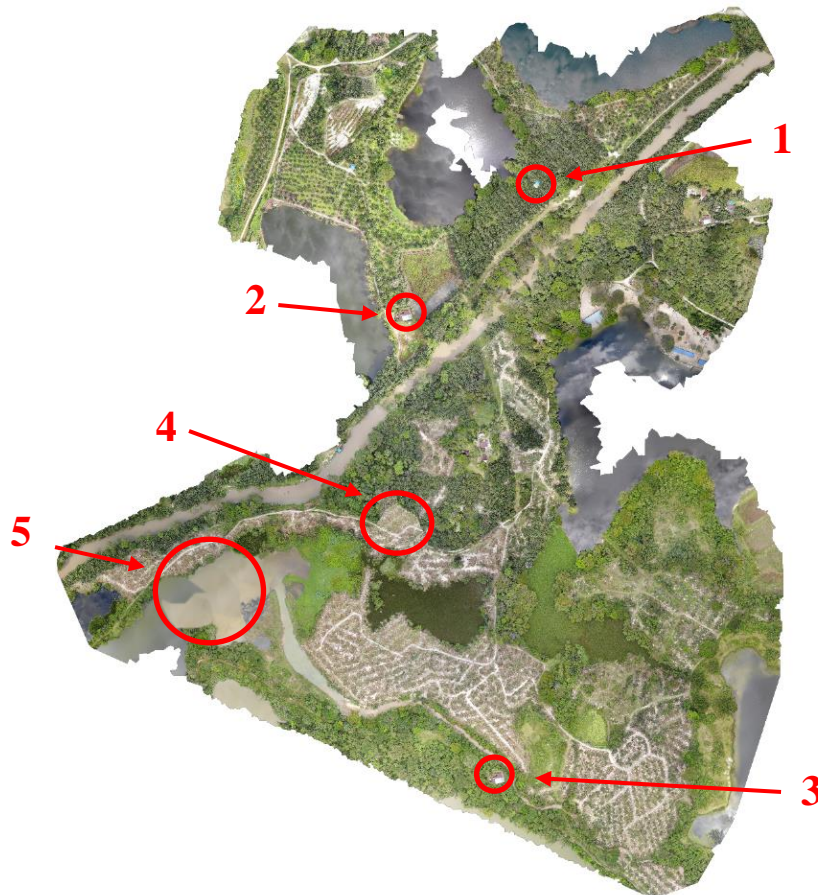


Figure 4.18: Edited Orthophoto of Plot_BC.

Discussions above have proved that the algorithm is able to detect changes. What if there are no changes? The drone had taken three Kuala Selangor rural area datasets on a different date, 14th January, 15th January and 17th January 2021. Figures 4.20, 4.21 show the result of change detection.



Figure 4.19: Plot_BC Edited Orthophoto with Highlighted Changes.



Figure 4.20: Kuala Selangor Change Map of 14th January and 15th January.



Figure 4.21: Kuala Selangor Change Map of 14th January and 17th January.

The results show that there are many changes. After analysis, the reason for these changes is found. The changes are due to the sunlight. A small section is cropped out to show the problem as shown in figure 4.22.



Figure 4.22: Cropped Image from 14th January (Left) and 17th January (Right).

Both images were taken at 2:30 pm. However, the image on the right has the occurrence of shadow, but the left does not. This phenomenon had created uncertainty for change detection. One solution is proposed to solve this false positive issue. The solution is stacking the change maps and carrying out the “bitwise_and” operation. The “bitwise_and” will compute the bitwise conjunction of the two arrays and create an output array. 1 and 1 will equal 1. 0 and 1 will become 0. 0 and 0 will remain 0. Only changes that occur in all change maps will remain. The others will count as false positives and be removed.

Figure 4.23 shows the output of such an algorithm. It is by combining the change map in figure 4.20 and figure 4.21.



Figure 4.23: New Change Map by “Bitwise And” Operation.

CHAPTER 5

CONCLUSIONS AND RECOMMENDATIONS

5.1 Conclusions

In a nutshell, the three objectives of the project are achieved. First, create the flight plans for the drone mapping mission. DJI Mavic 2 Enterprise Dual is selected as the drone for the surface surveillance. The drone will carry out the mapping mission via DJI Pilot periodically based on the flight plans. A total of 11 flight plans for the area of interest was created. Once the drone finishes the mapping mission, the drone needs to connect to a computer. A software will sort the images according to their coordinate autonomously. Once the mapping mission for all plots is completed and all images are transferred to the computer, the images can be used to reconstruct the orthophoto or so called 2D map through WebODM. The WebODM is set up at the UTAR server.

Second, carry out image reconstruction using aerial footage to create 2D and 3D maps. The parameters for the reconstruction are dem-resolution: 15, ignore-gsd: true, min-num-features: 20000, orthophoto-resolution: 15, skip-3dmodel: true, texturing-data-term: area. This setting creates the best orthophoto for the area of interest, which is the rural area around UTAR Kampar which is mainly covered by trees and green vegetation. The skip-3dmodel setting is to minimise the reconstruction time for the orthophoto. The software will only generate a 2.5D model since only orthophoto is used for the change detection. The reason for not taking 3D maps into consideration is due to their poor quality. The area is full of trees which is very difficult to reconstruct the 3D model. The point cloud of the area will still be generated. The skip-3dmodel setting can be turned off as well, and it would not affect the result at all.

Lastly, develop software to identify anomalies in the area under surveillance. After obtaining two orthophotos from different timestamps, the change detection can be carried out. The change detection is done by image registration followed by PCA and K-mean clustering on the “difference image” to cluster out changes and non-changes. A cluster of four is used for the K-mean clustering to minimise the noises and false-positive detection. The cluster whose

pixels have the highest average value will be the anomalies and a change map will be generated. The result is quite promising, but it still has a weakness. The change detection takes only the orthophoto, which causes the algorithm unable to detect changes which have a very similar RGB value.

5.2 Recommendations for Future Work

The accuracy of the drone is still not high enough. Real-time kinematics (RTK) base station is recommended to be implemented in this project. The accuracy of the drone positioning can increase to centimetre level. Theoretically, it will increase the result of the orthophoto as well. Besides, ground control points (GCPs) are also recommended to be implemented in this project. GCPs are the fiducial of the orthophoto. When used correctly, GCPs greatly improve the accuracy of the orthophoto. It helps to ensure that the longitude and latitude of any point on the map corresponds accurately with actual GPS coordinates.

In addition, more automation can be created as well. In the current stage of development, most of the parts in this project do not require human intervention already. However, there are still some parts that require human control. It is still not a fully autonomous system. For example, the operator needs to connect the drone to a computer to transfer the images. The process of connecting the drone and the computer can be removed via a wireless data transmission. The command of transferring images may be triggered once the drone is returned home.

Lastly, the algorithm of the change detection. The algorithm is good enough but still can be improved. As mentioned above, the algorithm is unable to detect changes which have a very similar RGB value. A 3D model or DTM can be taken into consideration when doing change detection. Perhaps the quality of the 3D model is increased with the help of RTK base station and GCPs.

REFERENCES

- Bruzzone, L. and Prieto, D., 2000. Automatic analysis of the difference image for unsupervised change detection. *IEEE Transactions on Geoscience and Remote Sensing*, 38(3), pp.1171-1182.
- Celik, T., 2009. Unsupervised Change Detection in Satellite Images Using Principal Component Analysis and K-Means Clustering. *IEEE Geoscience and Remote Sensing Letters*, 6(4), pp.772-776.
- Chapman, A., 2016. Types of Drones: Multi-Rotor vs Fixed-Wing vs Single Rotor vs Hybrid VTOL. DRONE, [online] (3). Available at: <<https://www.auav.com.au/articles/drone-types/>> [Accessed 18 August 2020].
- Davies, E., 2005. Machine Vision: Theory, Algorithms, Practicalities. Morgan Kaufmann Publishers.
- DJI. 2020. Mavic 2 Enterprise - Built To Empower. Destined To Serve - DJI. [online] Available at: <<https://www.dji.com/mavic-2-enterprise>> [Accessed 26 August 2020].
- DronesWatch., 2020. 5 Best Drones For Agriculture In 2020 – Buying Guide For Beginners - Droneswatch. [online] Available at: <<https://droneswatch.org/drones-for-agriculture/>> [Accessed 17 August 2020].
- Felzenszwalb, P. and Huttenlocher, D., 2004. Efficient Graph-Based Image Segmentation. *International Journal of Computer Vision*, 59(2), pp.167-181.
- Fischler, M. and Bolles, R., 1981. Random sample consensus: a paradigm for model fitting with applications to image analysis and automated cartography. *Communications of the ACM*, 24(6), pp.381-395.
- Gindraux, S., Boesch, R. and Farinotti, D., 2017. Accuracy Assessment of Digital Surface Models from Unmanned Aerial Vehicles' Imagery on Glaciers. *Remote Sensing*, 9(2), p.186.

Gong, M., Su, L., Jia, M. and Chen, W., 2014. Fuzzy Clustering With a Modified MRF Energy Function for Change Detection in Synthetic Aperture Radar Images. *IEEE Transactions on Fuzzy Systems*, 22(1), pp.98-109.

Greensted, A., 2010. Otsu Thresholding - The Lab Book Pages. [online] Labbookpages.co.uk. Available at: <<http://www.labbookpages.co.uk/software/imgProc/otsuThreshold.html>> [Accessed 26 August 2020].

Hartemink, A., 2005. Plantation Agriculture in the Tropics. *Outlook on Agriculture*, 34(1), pp.11-21.

Kar, A., 2017. Learning A Multi-View Stereo Machine. [online] The Berkeley Artificial Intelligence Research Blog. Available at: <<https://bair.berkeley.edu/blog/2017/09/05/unified-3d/>> [Accessed 26 August 2020].

Levin, D., 1998. The approximation power of moving least-squares. *Mathematics of Computation*, 67(224), pp.1517-1532.

Liu, Y., Zheng, X., Ai, G., Zhang, Y. and Zuo, Y., 2018. Generating a High Precision True Digital Orthophoto Map Based on UAV Images. *ISPRS International Journal of Geo-Information*, 7(9), p.333.

Lv, Z., Shi, W., Zhou, X. and Benediktsson, J., 2017. Semi-Automatic System for Land Cover Change Detection Using Bi-Temporal Remote Sensing Images. *Remote Sensing*, 9(11), p.1112.

Mathews, A., 2015. A Practical UAV Remote Sensing Methodology to Generate Multispectral Orthophotos for Vineyards. *International Journal of Applied Geospatial Research*, 6(4), pp.65-87.

Muja, M. and David Lowe, D., 2020. Fast Approximate Nearest Neighbors with Automatic Algorithm Configuration. In: *International Conference on Computer Vision Theory and Applications*.

Mysa.gov.my. n.d. *Remote Sensing Satellite Data Price List*. [online] Available at: <<http://www.mysa.gov.my/portal/index.php/remote-sensing-satellite-data-price-list>> [Accessed 26 August 2020].

Piza, E., Welsh, B., Farrington, D. and Thomas, A., 2019. CCTV surveillance for crime prevention. *Criminology & Public Policy*, 18(1), pp.135-159.

Qin, R., 2014. An Object-Based Hierarchical Method for Change Detection Using Unmanned Aerial Vehicle Images. *Remote Sensing*, 6(9), pp.7911-7932.

Rublee, E., Rabaud, V., Konolige, K. and Bradski, G., 2011. ORB: An efficient alternative to SIFT or SURF. 2011 International Conference on Computer Vision,.

Shao, P., Shi, W., He, P., Hao, M. and Zhang, X., 2016. Novel Approach to Unsupervised Change Detection Based on a Robust Semi-Supervised FCM Clustering Algorithm. *Remote Sensing*, 8(3), p.264.

Sikora, T., 2001. The MPEG-7 visual standard for content description-an overview. *IEEE Transactions on Circuits and Systems for Video Technology*, 11(6), pp.696-702.

Stars project. n.d. Images And Processing Routines. [online] Available at: <<https://www.stars-project.org/en/knowledgeportal/magazine/uav-technology/images-and-processing-routines/>> [Accessed 26 August 2020].

Tan, Y., Wang, J., Liu, J. and Zhang, Y., 2020. Unmanned Systems Security: Models, Challenges, and Future Directions. *IEEE Network*, 34(4), pp.291-297.

Tian, J., Reinartz, P., d'Angelo, P. and Ehlers, M., 2013. Region-based automatic building and forest change detection on Cartosat-1 stereo imagery. *ISPRS Journal of Photogrammetry and Remote Sensing*, 79, pp.226-239.

Toffanin, P., 2019. *Opendronemap: The Missing Guide*. 1st ed. UAV4GEO.

Ugliano, M., Bianchi, L., Bottino, A. and Allasia, W., 2015. Automatically detecting changes and anomalies in unmanned aerial vehicle images. 2015 IEEE

1st International Forum on Research and Technologies for Society and Industry
Leveraging a better tomorrow (RTSI).

Vacca, G., 2020. WEB Open Drone Map (WebODM) a Software Open Source to Photogrammetry Process WEB Open Drone Map (WebODM) a Software Open Source to Photogrammetry Process (10728) Giuseppina Vacca (Italy) FIG Working Week 2020 Smart surveyors for land and water man, pp. 10–14.

Vergouw, B., Nagel, H., Bondt, G. and Custers, B., 2016. Drone Technology: Types, Payloads, Applications, Frequency Spectrum Issues and Future Developments. Information Technology and Law Series, pp.21-45.

Vincent, L., 1993. Morphological grayscale reconstruction in image analysis: applications and efficient algorithms. IEEE Transactions on Image Processing, 2(2), pp.176-201.

Woebbecke, DM, Meyer, GE, Von Bargaen, K & Mortensen, DA., 1995. Shape features for identifying young weeds using image analysis, Transactions of the American Society of Agricultural Engineers, vol. 38, no. 1, pp. 271-281.

Xuan, W., 2011. Topographical Change Detection from UAV Imagery Using M-DSM Method. Communications in Computer and Information Science, pp.596-605.

Yang, H., Lee, Y., Jeon, S. and Lee, D., 2017. Multi-rotor drone tutorial: systems, mechanics, control and state estimation. Intelligent Service Robotics, 10(2), pp.79-93.

APPENDICES

APPENDIX A: DJI Mavic 2 Enterprise Dual Specification

Specs

Aircraft

Takeoff Weight(Without Accessories)

Zoom Edition:905 g

Dual Edition:899 g

Max Takeoff Weight

1100 g

Dimensions(L×W×H)

Folded : 214×91×84 mm

Unfolded: 322×242×84 mm

Unfolded+Spotlight : 322×242×114 mm

Unfolded+Beacon : 322×242×101 mm

Unfolded+Speaker : 322×242×140 mm

Diagonal Length

354 mm

Max Ascent Speed

5 m/s (S-mode⁽¹⁾)

4 m/s (P-mode)

4 m/s (S-mode with accessories⁽¹⁾)

4 m/s (P-mode with accessories)

Max Descent Speed

3 m/s (S-mode⁽¹⁾)

3 m/s (P-mode)

Max Speed (near sea level, no wind)

72 kph (S-mode , without wind)

50 kph (P-mode , without wind)

Max Service Ceiling Above Sea Level

6000 m

Max Flight Time (no wind)

31 min (at a consistent speed of 25 kph)

Max Hovering Time (no wind)

29 min

27 min (with beacon turned on)

28 min (with beacon turned off)

22 min (with spotlight turned on)

26 min (with spotlight turned off)

25 min (with speaker turned on)

26 min (with speaker turned off)

Max Wind Speed Resistance

29–38 kph

Max Tilt Angle

Max Angular Velocity

200°/s (S-Mode)
 100°/s (P-Mode) 200°/s (S-Mode)
 100°/s (P-Mode)

Operating Temperature Range

-10°C to 40°C

GNSS

GPS+GLONASS

Hovering Accuracy Range

Vertical:
 ±0.1 m (with Vision Positioning)
 ±0.5 m (with GPS Positioning)
 Horizontal: ±0.3m (with Vision Positioning)
 ±1.5 m (with GPS Positioning)

Operating Frequency

2.400 - 2.4835 GHz
 5.725 - 5.850 GHz

Transmission Power (EIRP)

2.400 - 2.4835 GHz
 FCC : ≤26 dBm
 CE : ≤20 dBm
 SRRC : ≤20 dBm
 MIC : ≤20 dBm
 5.725-5.850 GHz
 FCC : ≤26 dBm
 CE : ≤14 dBm
 SRRC : ≤26 dBm

Internal Storage

24 GB

M2ED Thermal Camera**Sensor**

Uncooled VOx Microbolometer

Lens

HFOV: 57°
 Aperture: f/1.1

Sensor Resolution

160×120

Pixel Pitch

12 μm

Spectral Band

8-14 μm

Image Size [2]

640×480 (4:3);
 640×360 (16:9)

Still Photography Modes

Single shot
 Burst shooting: 3/5/7 frames

<https://www.dji.com/mavic-2-enterprise/specs>

Accuracy

High Gain: Max $\pm 5\%$ (typical)
 Low Gain: Max $\pm 10\%$ (typical)

Scene Range

High Gain: -10° to $+140^{\circ}\text{C}$
 Low Gain: -10° to $+400^{\circ}\text{C}$

Photo

JPEG

Video

MP4, MOV (MPEG-4 AVC/H.264)

M2ED Visual Camera

Sensor

1/2.3" CMOS; Effective pixels: 12M

Lens

FOV: approx. 85°
 35 mm format equivalent: 24 mm
 Aperture: f/2.8
 Focus: 0.5 m to ∞

ISO Range

Video: 100-12800 (auto)
 Photo: 100-1600 (auto)

Max Image Size

4056 \times 3040 (4:3) ; 4056 \times 2280 (16:9)

Still Photography Modes

Single shot
 Burst shooting: 3/5/7 frames
 Interval (2/3/5/7/10/15/20/30/60 s)

Video Recording Modes

4K Ultra HD : 3840 \times 2160 30p
 2.7K : 2688 \times 1512 30p
 FHD : 1920 \times 1080 30p

Max Video Bitrate

100 Mops

Photo

JPEG

Video Format

MP4 , MOV (MPEG-4 AVC/H.264)

M2E Camera

Sensor

1/2.3" CMOS ;
 Effective pixels: 12 Megapixels

Lens

Auto focus at : 0.5 - ∞

ISO Range

Video :
100-3200
Photo :
100-1600(Auto)
100-12800(Manual)

Shutter Speed

8-1/8000s

Still Image Size

4000×3000

Still Photography Modes

Single shot
Burst shooting: 3/5/7 frames
Auto Exposure Bracketing (AEB): 3/5 bracketed frames at 0.7 EV Bias
Interval (JPEG: 2/3/5/7/10/15/20/30/60s RAW:5/7/10/15/20/30/60s)

Video Resolution

4K: 3840×2160 24/25/30p
2.7K: 2720×1530 24/25/30/48/50/60p
FHD: 1920×1080 24/25/30/48/50/60/120p

Max Video Bitrate

100 Mbps

Supported File System

FAT32(≤ 32 GB) ; exFAT(> 32 GB)

Photo Format

JPEG , DNG (RAW)

Video Format

MP4 / MOV (MPEG-4 AVC/H.264)

Gimbal

Mechanical Range

Tilt: -135 – +45°
Pan: -100 – +100°

Controllable Range

Tilt: -90 – +30°
Pan: -75 – +75°

Stabilization

3-axis (tilt, roll, pan)

Max Control Speed (tilt)

120°/s

Angular Vibration Range

±0.005°

Sensing System

Sensing System

<https://www.dji.com/mavic-2-enterprise/specs>

Precision Measurement Range: 0.5 - 20 m
 Detectable Range: 20 - 40 m
 Effective Sensing Speed: $\leq 14\text{m/s}$
 FOV: Horizontal: 40°, Vertical: 70°

Backward

Precision Measurement Range: 0.5 - 16 m
 Detectable Range: 16 - 32 m
 Effective Sensing Speed: $\leq 12\text{m/s}$
 FOV: Horizontal: 60°, Vertical: 77°

Upward

Precision Measurement Range: 0.1 - 8 m

Downward

Precision Measurement Range: 0.5 - 11 m
 Detectable Range: 11 - 22 m

Sides

Precision Measurement Range: 0.5 - 10 m
 Effective Sensing Speed: $\leq 8\text{m/s}$
 FOV: Horizontal: 80°, Vertical: 65°

Operating Environment

Forward, Backward and Sides:

Surface with clear pattern and adequate lighting (lux > 15)

Upward:

Detects diffuse reflective surfaces (>20%)
 (walls, trees, people, etc.)

Downward:

Surface with clear pattern and adequate lighting (lux > 15)

Detects diffuse reflective surfaces (>20%)
 (walls, trees, people, etc.)

Remote Controller

Operating Frequency

2.400 - 2.483 GHz; 5.725 - 5.850 GHz

Max Transmission

Distance (Unobstructed, free of interference)

2.400 - 2.483 GHz; 5.725 - 5.850 GHz

FCC: 10000 m

CE: 6000 m

SRRC: 6000 m

MIC: 6000 m

Operating Temperature Range

0°C to 40°C

Transmitter Power (EIRP)

2.4 - 2.4835 GHz

FCC : $\leq 26\text{ dBm}$; CE : $\leq 20\text{ dBm}$; SRRC : $\leq 20\text{ dBm}$ MIC : $\leq 20\text{ dBm}$

5.725 - 5.850 GHz

FCC : $\leq 26\text{ dBm}$; CE : $\leq 14\text{ dBm}$; SRRC : $\leq 26\text{ dBm}$

Battery

3950mAh

Charging Time

<https://www.dji.com/mavic-2-enterprise/specs>

1800mA = 3.83V

Mobile Device Holder

Thickness Supported: 6.5-8.5 mm , Max length: 160 mm

RC Size

Folded : 145×80×48 mm (L×W×H)

Unfolded: 190×115×100 mm (L×W×H)

Supported USB port types

Lightning, Micro USB (Type-B), USB Type-C™

Intelligent Flight Battery

Capacity

3850 mAh

Voltage

15.4V

Max Charging Voltage

17.6V

Battery Type

LiPo

Energy

59.29 Wh

Net Weight

297 g

Charging Temperature

5°C - 40°C

Operating Temperature Range

-10°C to 40°C

Heating Methods

Manual Heating ; Auto Heating

Heating Temperature

-20°C to 6°C

Heating duration

600s (Max)

Heating Power

35W (Max)

Charging Time

90 min

Max Charging Power

80W

Charger

Input

100-240V , 50-60Hz , 1.8A

<https://www.dji.com/mavic-2-enterprise/specs>

USB: 5 V – 2 A

Voltage
17.6±0.1V

Rated Power
60W

M2E Beacon

Dimensions
68x40x27.8 mm

Port Type
USB Micro-B

Power
Avg. 1.6W

Controllable Range
5000 m

Light intensity
Min Angle : 55 cd ;
Light intensity : 157 cd

M2E Spotlight

Dimensions
68x60x41 mm

Port Type
USB Micro-B

Operating Range
30 m

Power
Max 26W

Illuminance
FOV17°, Max : 11lux @ 30m Straight

M2E Speaker

Dimensions
68x55x65 mm

Port Type
USB Micro-B

Power
Max 10W

Decibel
100 db @ 1 meter distance

Bitrate
16 kbps

<https://www.dji.com/mavio-2-enterprise/specs>

OcuSync 2.0

Mobile App
DJI PILOT

Live View Quality
Remote Controller:
720p@30fps / 1080p@30fps

Max Live View Bitrate
40 Mbps

Latency
120 - 130 ms

Required Operating Systems
ios 10.0 or later Android 5.0 or later

Supported SD Cards

Supported SD Cards
Micro SD™
Supports a microSD with capacity of up to 128 GB. A UHS-I Speed Grade 3 rating microSD card is required.

Footnotes

Footnotes

[1] Remote controller required.

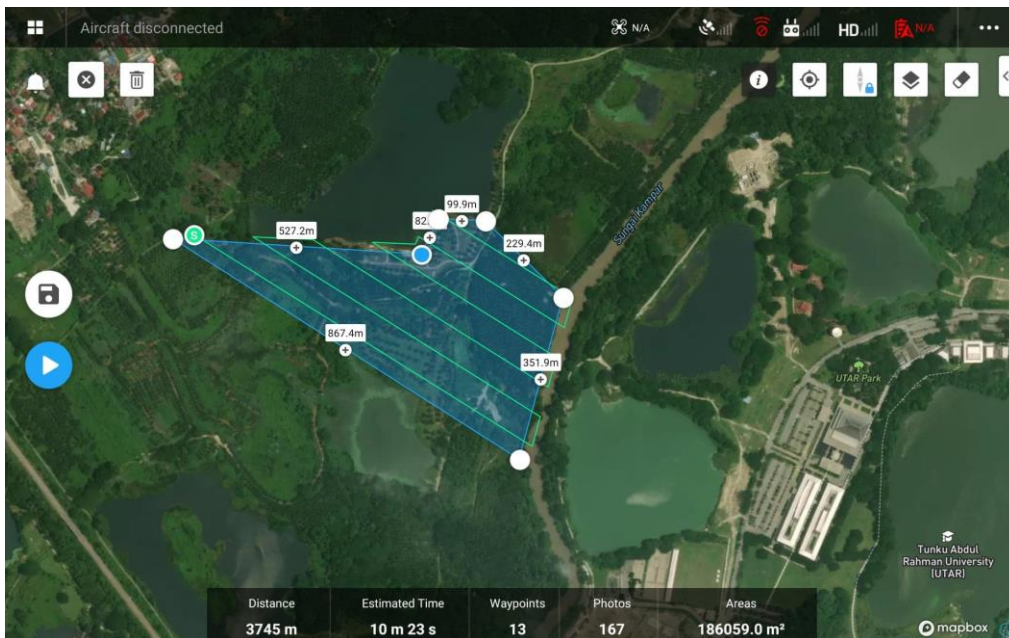
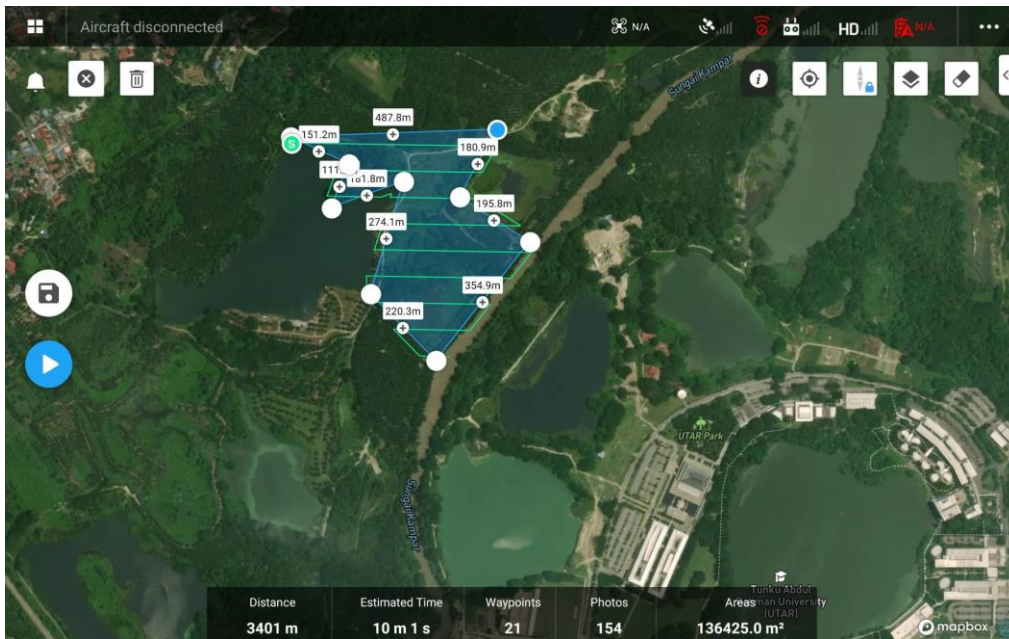
[2] Due to real-time digital enhancements, the photo and video size of the thermal data is larger than the sensor's native resolution.

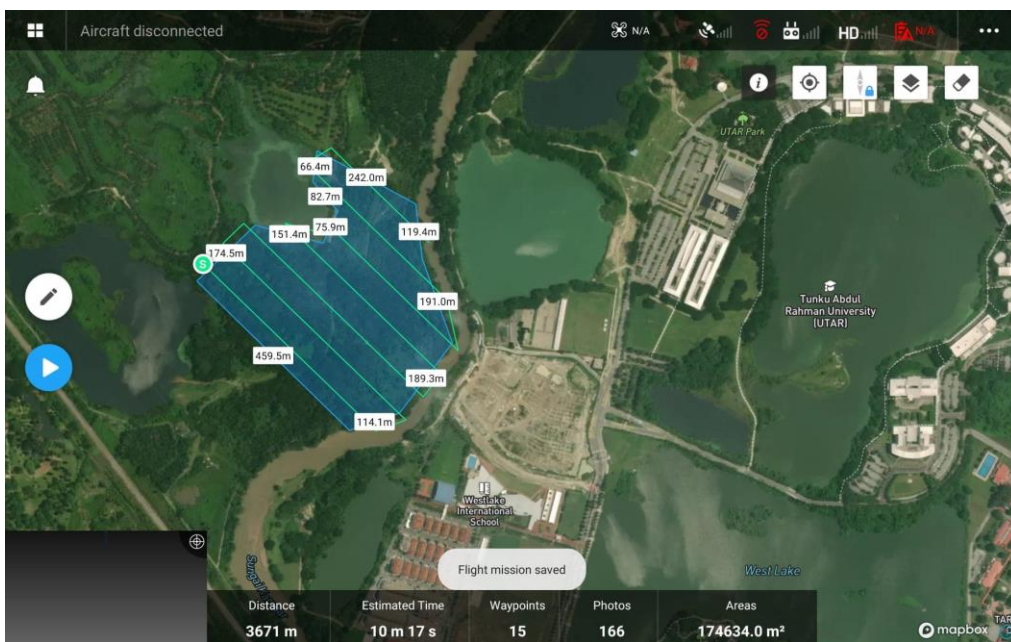
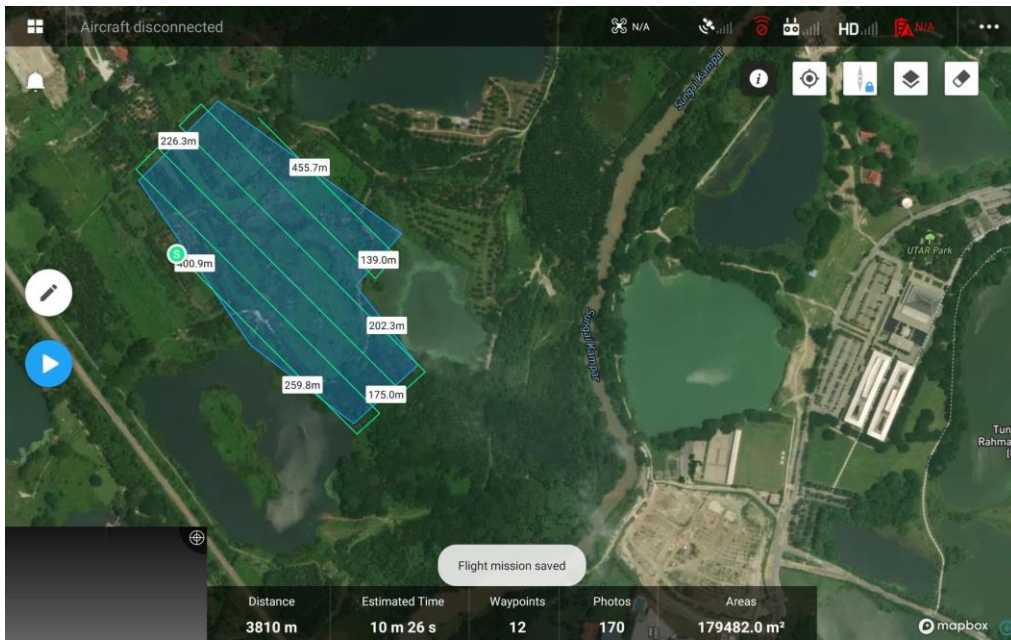
[3] Omnidirectional Obstacle Sensing includes left/right, up/down, and forward/backward obstacle sensing. Sensing for left/right directions is only ActiveTrack or Tripod Mode. Omnidirectional Obstacle Sensing does not fully cover the circumference of a 360-degree arc. And left and right obstacle system only works in specific modes and environments. DJI warranty does not cover any loss caused by crashing when flying left or right, even when Tripod mode is activated. Please be aware of your surroundings and App notifications when operating the Mavic 2 to ensure safety. These specs determined through tests conducted with the latest firmware. Firmware updates can enhance performance, so updating to the latest firmware is recommended."

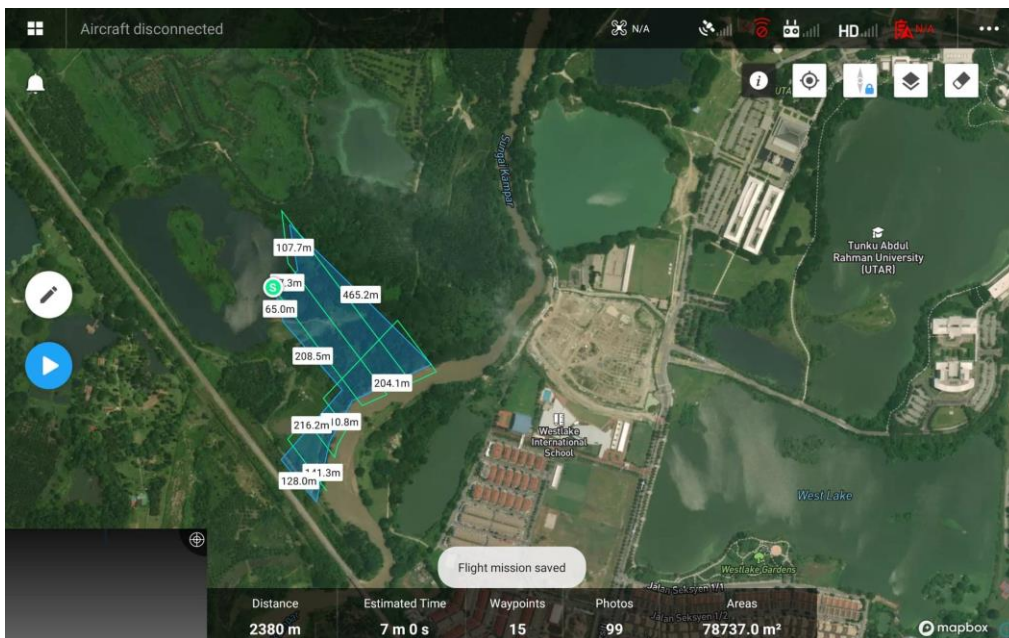
[4] These specs have been determined through tests conducted with the latest firmware. Firmware updates can enhance performance, so updating firmware is highly recommended."

APPENDIX B: Flight Plans of the Drone

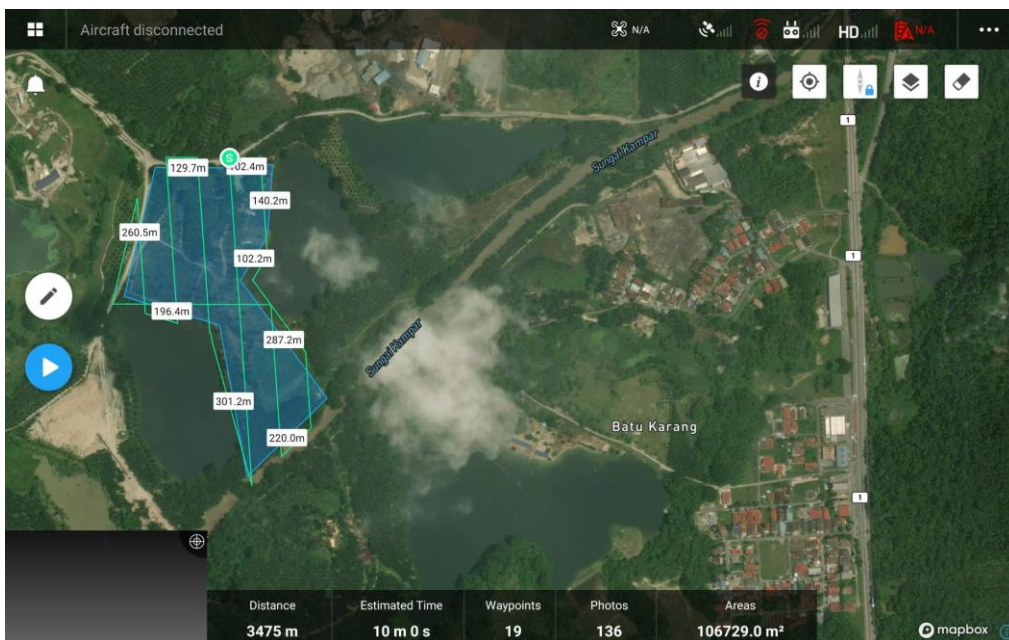
Plot A

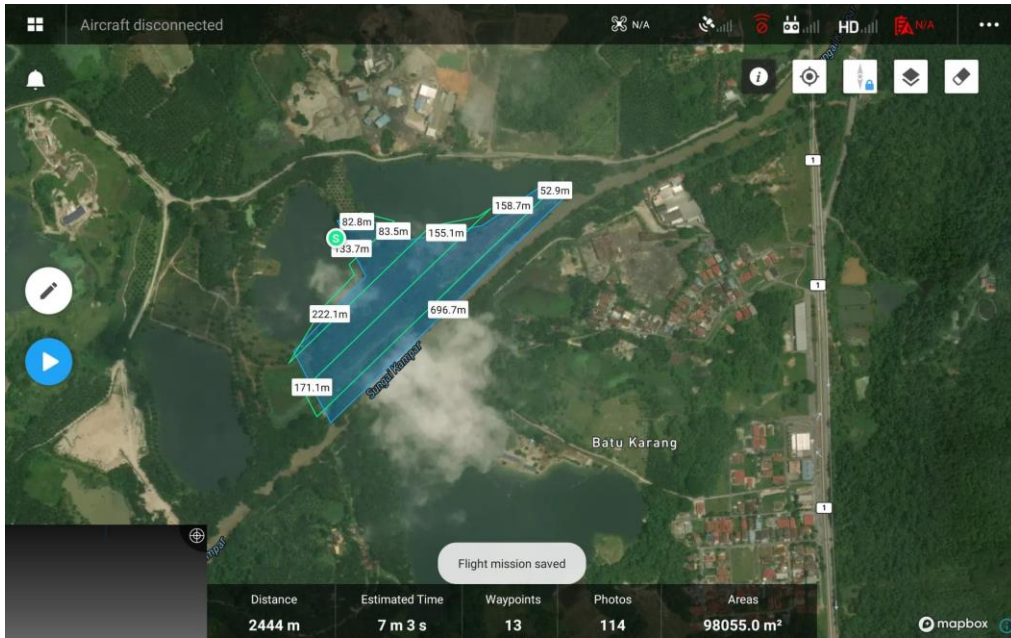




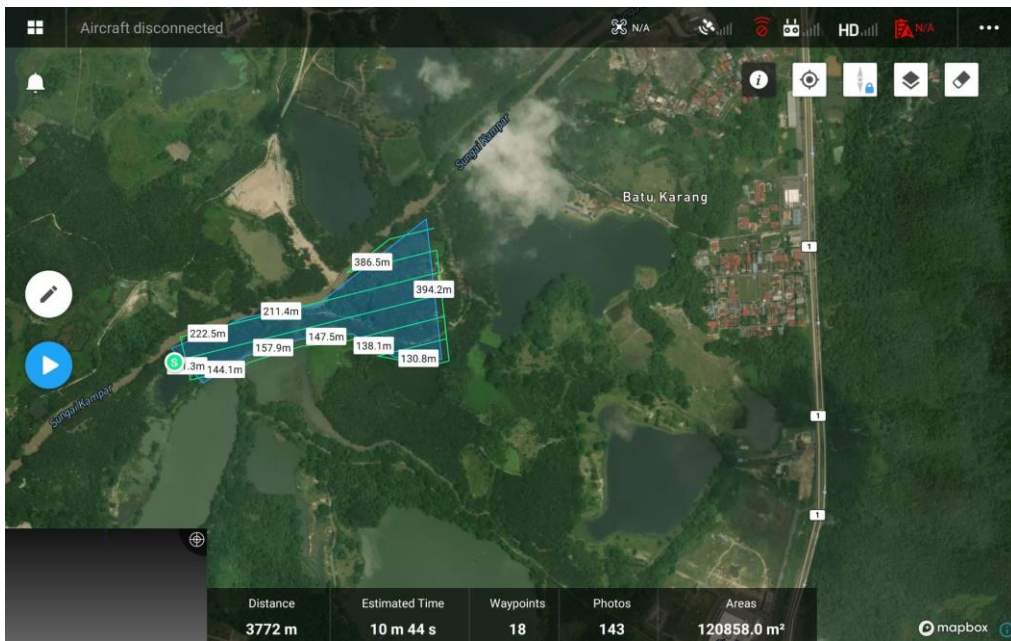


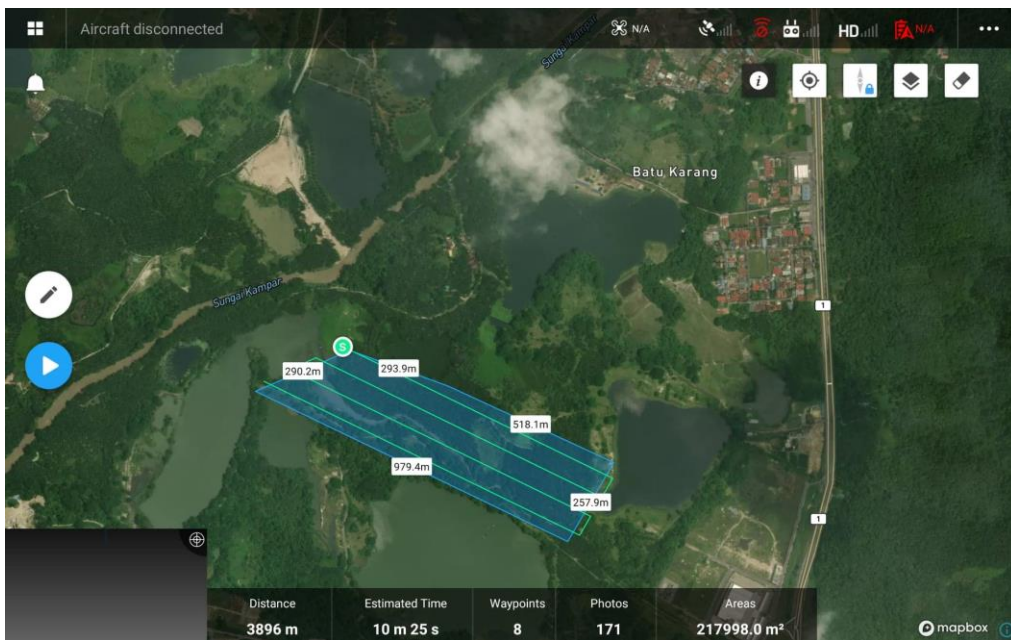
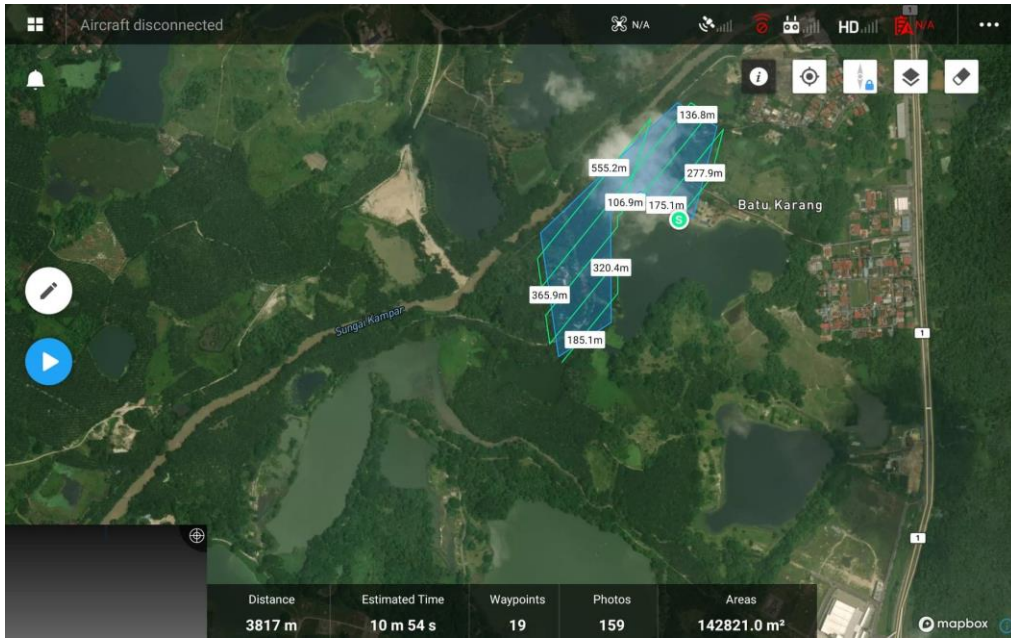
Plot B

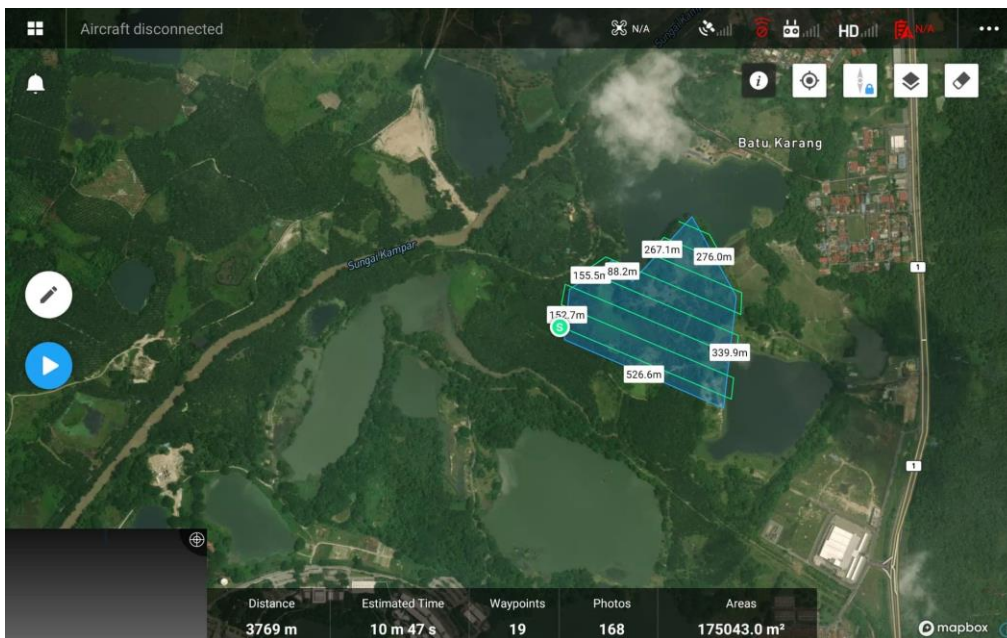




Plot C







APPENDIX C: Flight Planning of Operation Area

PART A - Illustration of the entire activity area.

The Accountable Manager shall submit the entire activity area using a map application (e.g. Google Map etc.) with annotation of **take-off / landing site**.

The entire operating zone has to be marked and its GPS co-ordinates (4 corners) taken as suggested in the list below:

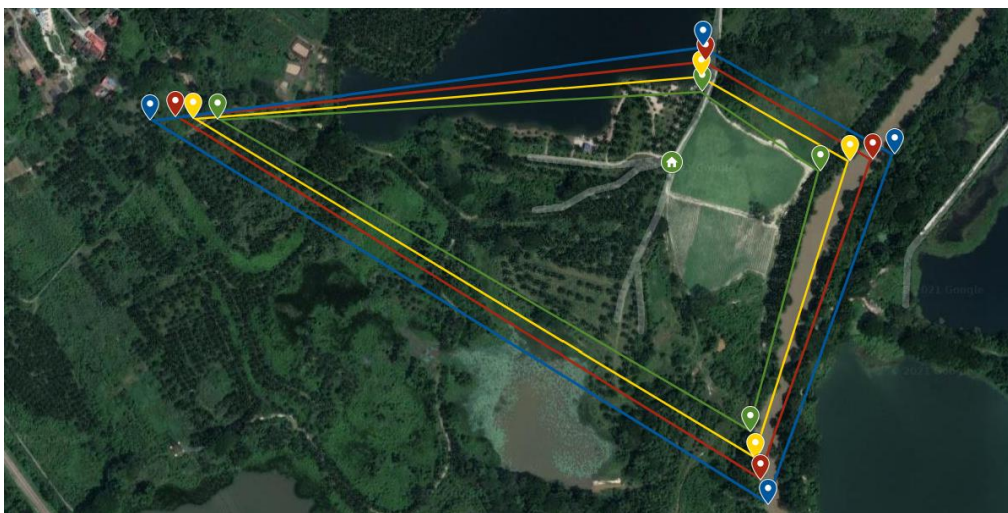
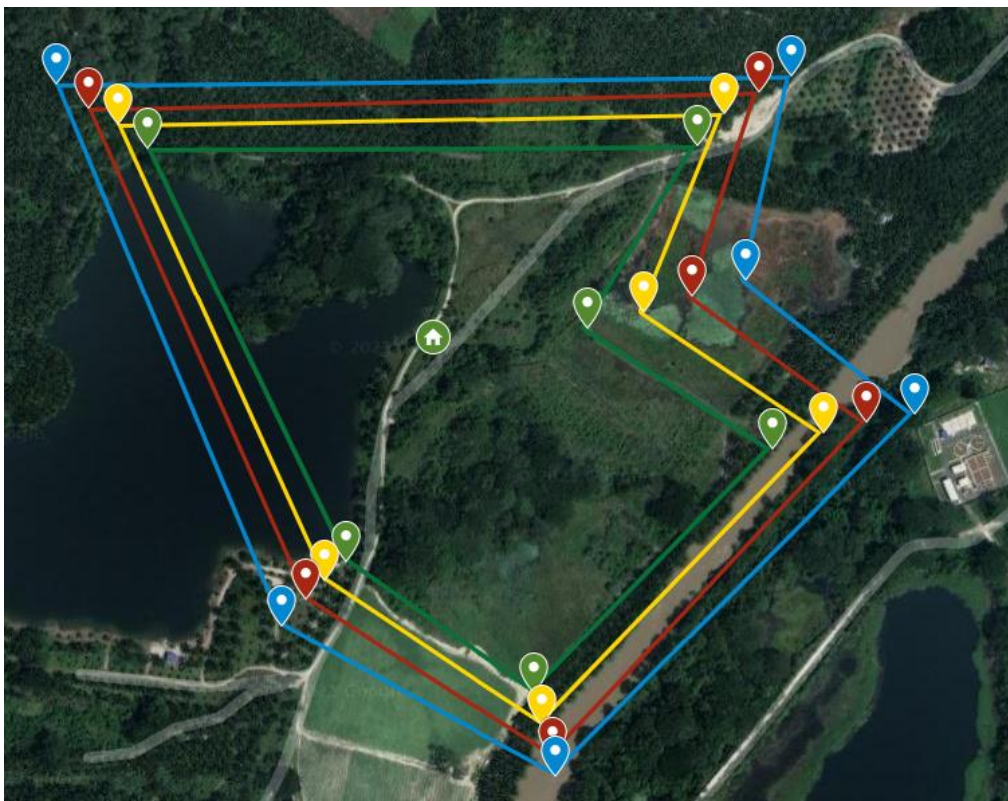
Activity zone (Green Zone): Activity area for all intended RPA flight-phases (Take-Off, Mid-Flight, Approach and Landing).

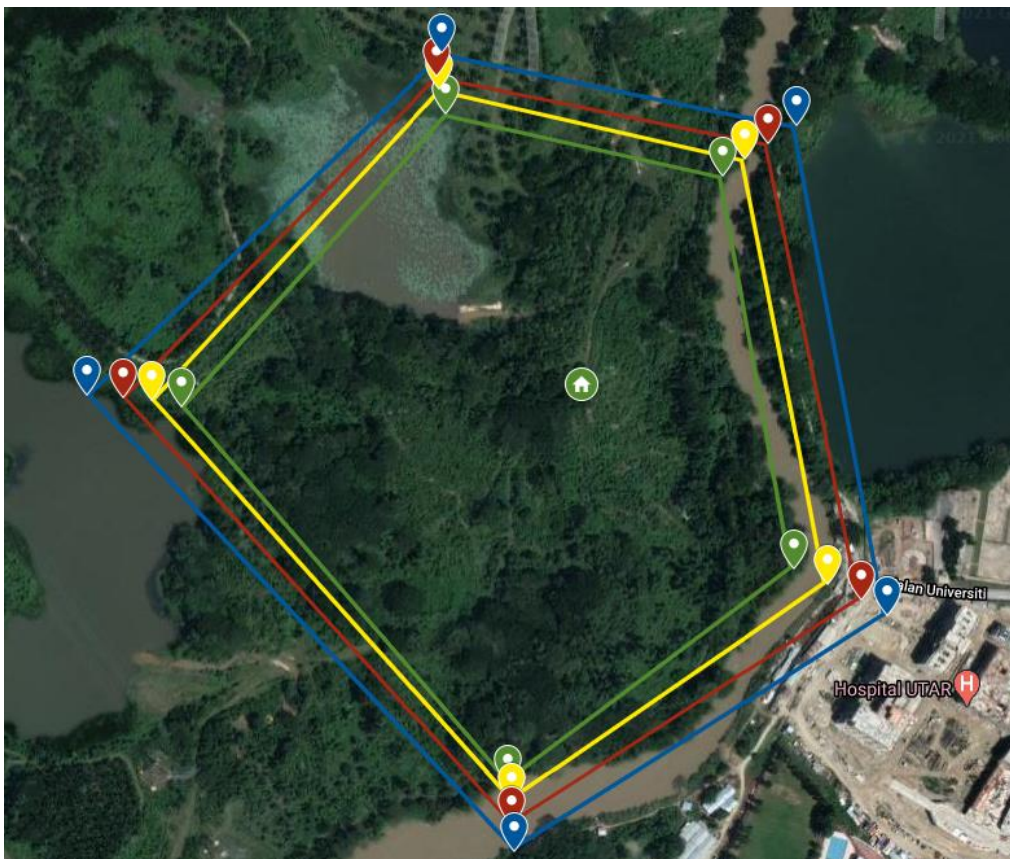
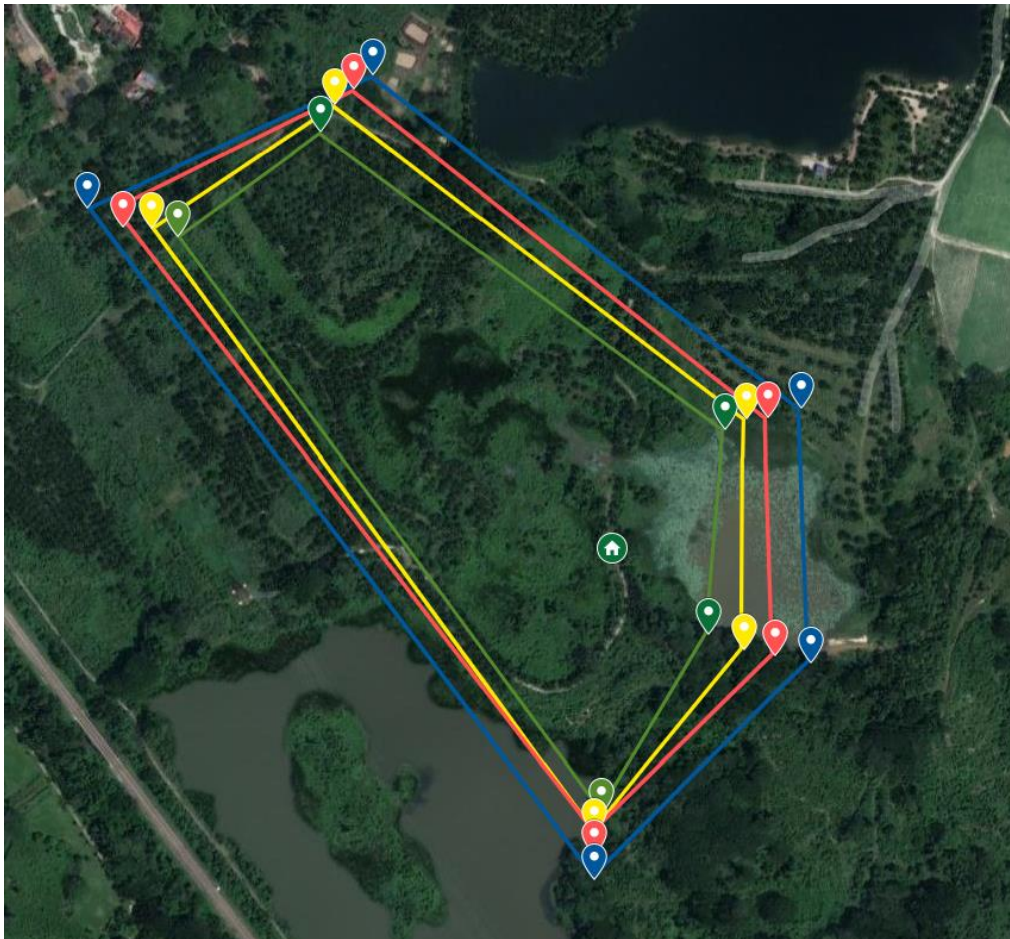
Geo-fencing zone (Yellow Zone): If the RPA strays from formation/flight path and encounters this boundary, flight control system instructs the RPA to return to home (fixed wing or multi-rotors) or hover in stationary (multi-rotors). Remote Pilot shall assume manual control and bring the RPA back to safety.

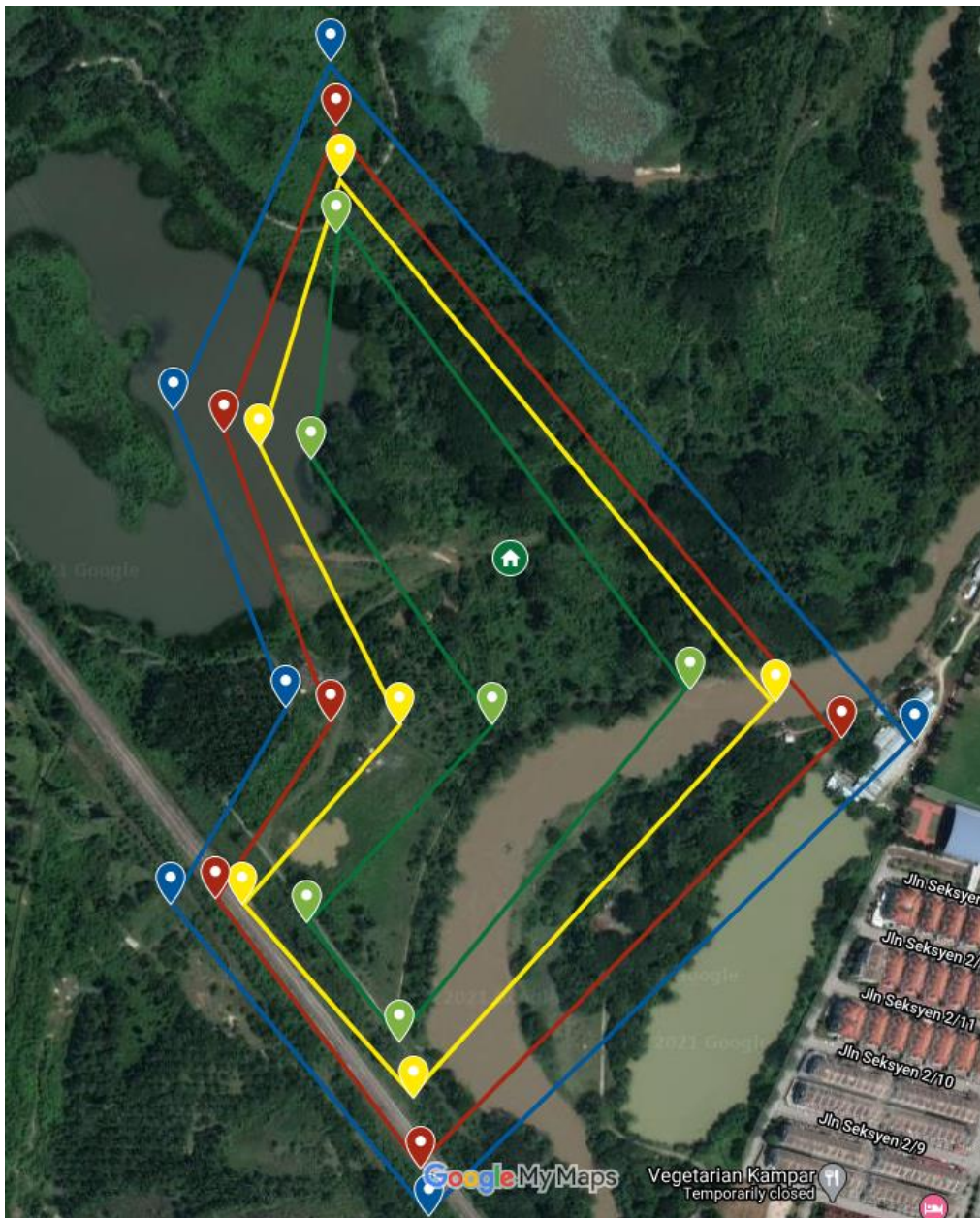
Risk zone (Red Zone): In rare case of malfunction or unexpected weather, if the RPA encounters this boundary, flight control system instructs the RPA to land or cut-off power to motor immediately. This is a safety measure (failsafe) to prevent fly-away or further motorized travel of the RPA.

Boundary zone (Blue Zone): This area shall be monitored by visual observers for safe operations during take-off, mid-flight, approach and landing flight phases. This area acts as a worst-case fall zone in case of UAS entering Risk Zone due to rare malfunction.

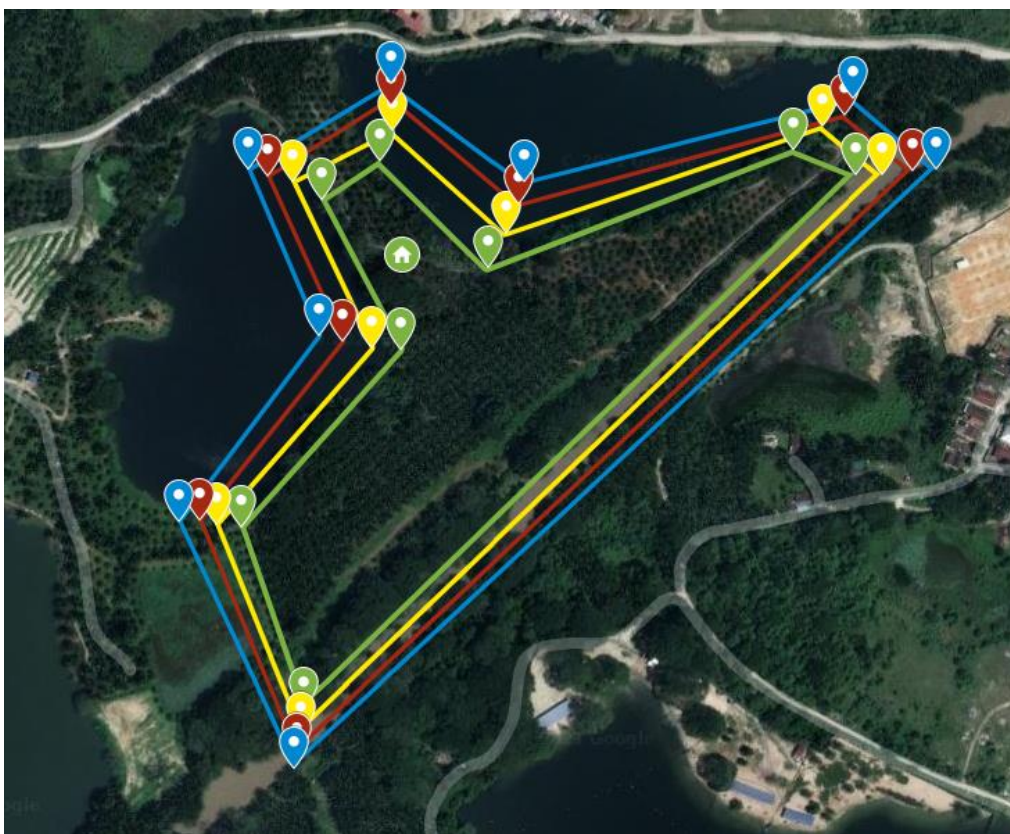
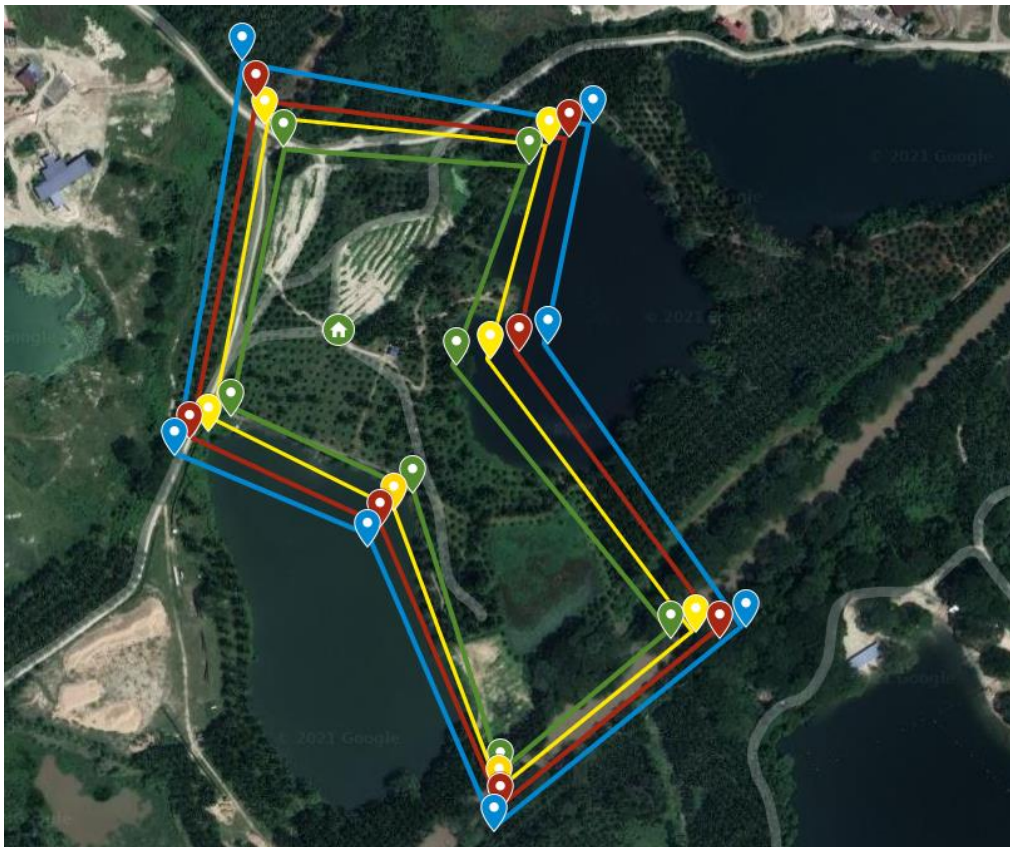
Plot A







Plot B



Plot C

